VOLUME 20, 1958/59, No. 8 pp. 209-244 Published 23th March 1959

Philips Technical Review

DEALING WITH TECHNICAL PROBLEMS
RELATING TO THE PRODUCTS, PROCESSES AND INVESTIGATIONS OF
THE PHILIPS INDUSTRIES

THE SCINTILLATION COUNTER

by J. A. W. van der DOES de BYE.

621.387.464

The scintillation counter — the most efficient gamma-ray counter now available — is finding ever-increasing application in medicine and industry as well as in physics. In many hospitals, its use in conjunction with radioisotopes ("tracers") has become a part of routine diagnostic practice.

A description is given below of the scintillation counter marketed some time ago by Philips. The article briefly discusses the physical principles underlying the operation of a scintillation counter, and the disturbing effects of inherent noise and background radiation which must be reckoned with both by the designer and by the user of such equipment.

The method of measuring the intensity of high-energy radiation by means of the scintillation effect, i.e. the property of some substances to emit flashes of light when exposed to such radiation, is one of the earliest known to nuclear physics. The method originally consisted in counting the number of scintillations produced by α particles incident on a zinc-sulphide screen; the observer viewed the screen under a magnifying glass or microscope and counted the scintillations visually. With the development of the Geiger-Müller counter in the thirties, which, with electronic scalers, made it possible to count very many more particles (quanta) per second and was moreover suitable for detecting β and γ radiation, the scintillation method fell into disuse. In the last ten years, however, in conjunction with the photomultiplier tube, it has acquired a new lease of life as the *scintillation counter,* which is now an important and widely used monitoring instrument in the fields of nuclear physics and medicine.

The following remarks will serve to define roughly the position of the scintillation counter in relation to the other types of radiation detectors. As is known, the quanta and particles emitted by radioactive substances give rise to *ionization* and *excitation* in their passage through matter. The operation of the hitherto most widely used radiation detectors, viz. the ionization chamber, the proportional counter and the Geiger-Müller counter, is based solely on the ionization effect. These instruments are ideally suited for the detection of charged particles — the Geiger tube counts every charged particle — but not for the detection of gamma rays. Owing to their high penetrating power, there is a considerable chance of the gamma quanta passing right through the detector without causing any ionization, or excitation. In the Geiger counter the chance of an incident γ-quantum being counted is, within a wide energy range, of the order of magnitude of only 1%.

Since the chance of a γ-quantum being absorbed increases with the total mass of the absorbing medium, appreciable improvement in the situation could only be obtained by using instruments containing a substantial quantity of liquid or solid matter as detector. Attempts to construct ionization chambers filled with a liquid or solid proved successful in principle, but failed to lead to instruments that could be produced and used on a large scale [1]). A great step forward was made with the advent of the photomultiplier tube which, being a much more rapid detector than the human eye, made it possible to revert to the old scintillation method, i.e. to a method of detection based not on the accumulation of liberated charges but on the localized luminescence caused in some substances by ionization and excitation. (The ordinary photoelectric cell is also fast, but for other reasons is unsuitable.) Provided they are optically transparent, scintillating materials of relatively large volume can be used without impairing the detectability of the light flashes, enabling a gamma-ray counter to be built that can count a high percentage of the incident quanta, even of very hard radiations (high quantum counting efficiency).

---

[1]) A discussion of the properties of various materials that can be used in an ionization chamber of the crystal-counter type is given by F. C. Champion, Progr. nucl. Phys. 3, 159-176, 1953.

A scintillator at present commonly used is sodium iodide, activated with a small amount (about 1%) of thallium. For some years now it has been possible to make single crystals of this substance, thus meeting the two requirements of transparency and large mass. The fact that NaI is extremely hygroscopic, however, entails special measures in mounting the crystal.

In regard to its "dead time", i.e. the time which must elapse after a count before the next quantum can be counted, the scintillation counter is far superior to the Geiger counter and is roughly on a par with the proportional counter. The dead time of a scintillation counter ²) fitted with an NaI(Tl) crystal is at most $2\frac{1}{2}$ μsec. Finally, it is also possible with the scintillation method to measure the *energy* of the incident quanta, that is to say to construct *scintillation spectrometers*.

Its high quantum counting efficiency for gamma rays makes the scintillation counter very suitable for applications involving the use of only small quantities of radioactive material. This is particularly the case where the material is administered to a patient for medical purposes, the object usually being to study the patient's metabolism. The property of some chemical compounds to concentrate in certain tissues may also be exploited; the tissues then become radiation sources and are as such detectable. With a narrow collimator, through which the scintillator "sees" only a small part of the object at a time, the size and shape of such tissues can be determined by scanning the object point by point.

Monitoring for radioactive contamination of the ground and of the human body also involves only slight amounts of radioactive material, and scintillation counters are therefore often employed in equipment for this purpose ³).

Scintillation counters are sometimes used instead of Geiger counters for the measurements on liquid samples occurring in medical and biological practice. The scintillation counters designed for such work often have a hollowed-out (well-type) crystal into which a test tube fits, so that a very large fraction of the total emitted γ radiation enters the crystal. Moreover, the position of the sample with respect to the crystal is not nearly so critical as when a flat crystal is used.

Many industrial applications are a variant of radiography with X-rays, being similarly based on the locally varying attenuation suffered by a beam of gamma rays in passing through an inhomogeneous body. The non-destructive testing of materials, as for example the detection of flaws in castings and controlling the thickness of sheet metal in a rolling mill, are often carried out with gamma rays, for which purposes the object is scanned with a scintillation counter. Prospecting for uranium ores with a portable scintillation counter is a familiar example of the geological applications.

In the following pages we shall describe the scintillation counter developed and marketed by Philips, and discuss the physical principles underlying its operation. We shall then consider disturbing effects, such as noise and background radiation, and conclude by touching briefly on the properties of scintillating materials other than NaI(Tl), the detecting of radiations other than gamma radiation, and scintillation spectrometry.

Description of the scintillation counter

The scintillating material, in the shape of a cube or cylinder, is mounted with one of its flat faces in good optical contact with the window of a photomultiplier tube, behind which is situated the photocathode. The electrons released from the photocathode by a light flash are attracted to a secondary-emitting electrode (dynode) which is maintained at a certain positive potential (about 150 V) with respect to the cathode. Each electron impinging on this dynode liberates a number of secondary electrons, which in their turn travel to the next dynode, and so on (*fig. 1*). The number of dynodes, i.e. the number of times this process is repeated, is about 10 in most commercially available photomultiplier tubes. This gives a tube gain of between 1 and 10 million times, making it possible to detect scintillations that liberate only one electron from the photocathode.

The current pulses at the output of the photomultiplier give rise to voltage pulses across the anode load. These are passed through a suitably designed amplifier, and the amplified pulses are fed via a *pulse-height discriminator* — a circuit preset to pass only those pulses that exceed a certain

---

²) A forthcoming article in this Review will deal with problems concerning the dead time of a scintillation counter in more detail than is possible here, and will also explain the reasons for the value mentioned above. For the dead time of the proportional counter see P. H. Dowling, C. F. Hendee, T. R. Kohler and W. Parrish, Philips tech. Rev. **18**, 262-275, 1956/57.

³) See e.g. A. Nemet, R. B. Stephens and W. A. Bayfield, Philips tech. Rev. **16**, 201-210, 1954/55.

height — to a scaling circuit. Each stage of the latter divides the number of pulses it receives by a certain factor — in the present instance 10. This is conveniently achieved by the use of decade scaler tubes [4]), from which the number of counted pulses in units, tens, hundreds, etc., can be read directly, each tube delivering one digit of this number. A block diagram of the arrangement is given in *fig. 2.* A photograph of the complete Philips scintillation counting equipment is shown in *fig. 3.* The counter is fitted with an NaI(Tl) crystal, which is mounted together with the multiplier tube (Philips 50 AVP) and the first amplifying stage (cathode-follower circuit) to form a *probe.* The latter is connected by a cable to the rack containing the rest of the equipment. This consists of a power pack which supplies the high tension for the multiplier tube (for 10 dynodes, about 1500 V), a pulse amplifier and a counting unit fitted with decade scaler tubes, which also functions as a fixed-level (non-variable) discriminator. The equipment allows the counting rate, i.e. the average number of quanta detected per unit time, to be determined either from the number of quanta counted within a given time, or from the time taken for the number of counts to reach a pre-set value, e.g. 10 000 [5]).

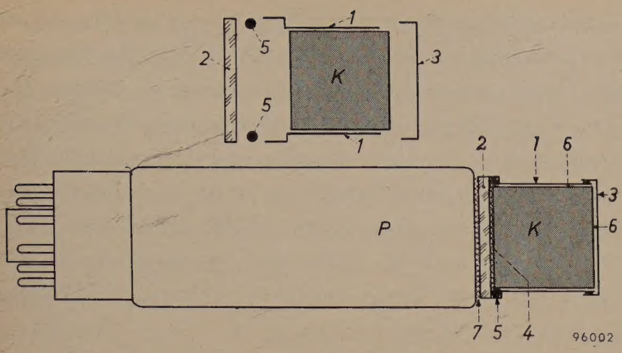

Fig. 1. Example of the way in which an NaI(Tl) crystal (K) can be mounted on the photomultiplier tube (P) in a scintillation counter. The crystal is hermetically sealed in a holder, which completely prevents the penetration of water vapour. *1* aluminium sleeve, *2* glass base, *3* aluminium cap cemented to the sleeve, *4* thin film of transparent viscous fluid, *5* rubber ring, *6* reflecting layer of MgO between aluminium wall and crystal, *7* fluid film as *4*. The two fluid films improve the optical contact between the crystal, the glass base and the tube window. The rubber ring separates the fluid from the MgO, which serves to increase the reflection from the walls.

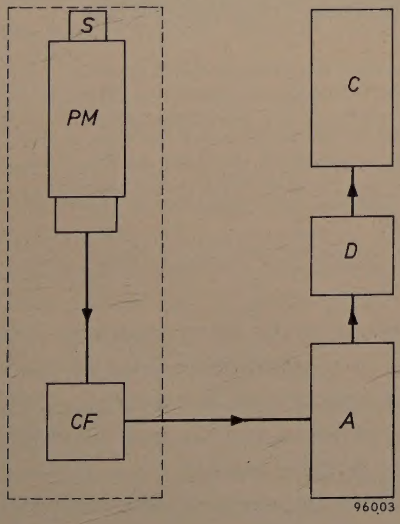

Fig. 2. Block diagram of a scintillation counter layout. *S* scintillator, *PM* photomultiplier tube, *CF* pre-amplifier, *A* pulse amplifier, *D* discriminator, *C* counting unit. Scintillator, photomultiplier tube and pre-amplifier are mounted together in a "probe".

The chance that the counter will register a gamma quantum entering the crystal is about 50% for quanta of 500 keV, 35% for quanta of 1 MeV and 25% for quanta of 2 MeV. In the case of soft gamma and X-ray quanta (10-50 keV) the chance is almost 100%. These values relate to a cylindrical crystal 2.5 cm in diameter and 2 cm in height. Crystals of other dimensions can also be mounted.

Processes occurring in the scintillation material

Before discussing the properties of the scintillation counter, we shall briefly review the processes that occur inside the scintillator. These are of two kinds, the first being the *absorption* of gamma quanta, which takes place in three ways, and the second the *emission of light* (the actual scintillation process).

Absorption of gamma rays

When a beam of mono-energetic gamma quanta passes through a layer of matter of thickness d, the intensity $I(d)$ of the emergent beam is given, as for X-rays, by the formula

$$I(d) = I(0)\, \mathrm{e}^{-\varrho\sigma d}, \quad . \; . \; . \; . \; . \quad (1)$$

where $I(0)$ is the intensity of the incident beam, ϱ the density of the material and σ the mass attenuation coefficient. If the product $\varrho\sigma$ is large, the material is strongly absorbent. The mass attenuation coefficient depends on the chemical composition of the absorber (but *not* on its state of aggregation) and on the energy E_0 of the incident gamma quanta.

The absorption of the gamma quanta may involve three distinct processes: the photo-electric effect, the Compton effect and pair production. The probability of these processes taking place varies with E_0, but differently in each case. Each process has its own mass attenuation coefficient, defined respectively as σ_f, σ_c and σ_p; the value of σ is the sum of the three. During these processes the energy of the gamma quantum is either wholly or partly converted into the kinetic energy of one or more electrons. If, then, a beam of mono-energetic gamma quanta is absorbed, the energy spectrum of these electrons is not mono-energetic (monochromatic), but fairly complex and partly continuous.

---

[4]) See e.g. A. J. W. M. van Overbeek, J. L. H. Jonker and K. Rodenhuis, Philips tech. Rev. 14, 313-326, 1952/53.

[5]) Cf. W. Parrish, Philips tech. Rev. 17, 206-221, 1955/56.

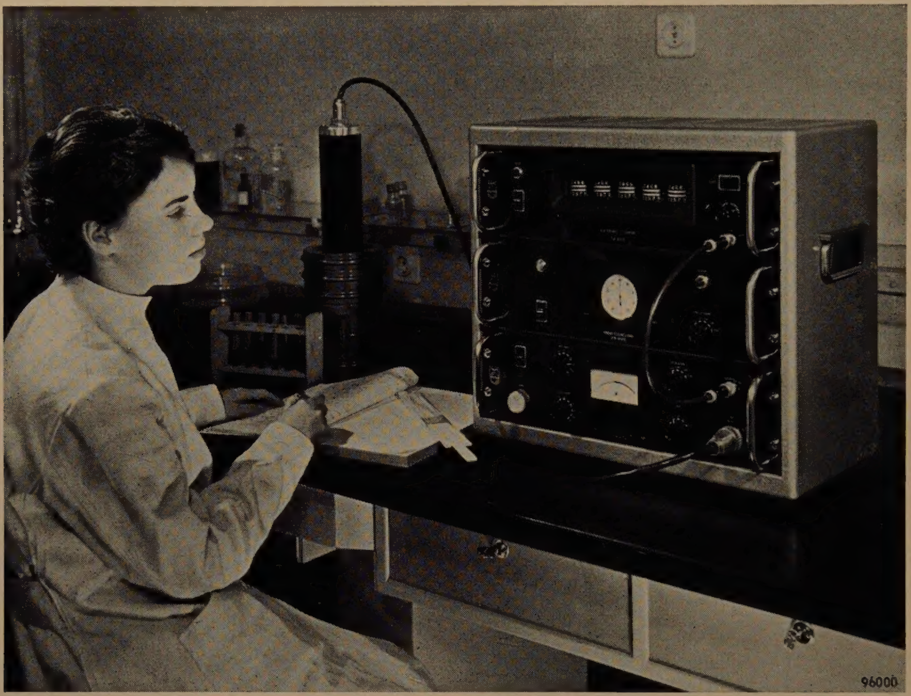

Fig. 3. The Philips scintillation counter in use. The upper part of the probe projects above a lead shield ("castle") at the bottom of which the radioactive specimen is situated. The probe is connected by a cable to the cabinet containing the rest of the electronic equipment. The bottom unit contains on the left the power pack for the photomultiplier tube (and to which a Geiger counter can also be connected) and on the right the pulse amplifier. The top unit contains the counting circuit, which also functions as pulse-height discriminator. The middle panel is fitted with a clock which indicates the time in which the apparatus has counted a pre-determined number of pulses.

The apparatus was developed to the production stage under the direction of Mr. A. Mooy.

In the first of the three processes — the *photo-electric effect* — an electron (usually a K electron) is ejected from its shell by the gamma quantum. The latter is thereby completely absorbed, i.e. the energy of the photo-electron is equal to the gamma energy minus the electron binding energy. When the electron configuration returns to its normal state — which it does in a very short time — the binding energy in question is emitted in the form of X-ray quanta or Auger electrons, or both. Any X-ray quanta emitted are in turn absorbed in their immediate surroundings, so that the quantum energy E_0 is entirely converted into electron kinetic energy. Since only the total electron energy is important for the scintillation process, we shall assume that we are concerned with a single electron of energy E_0. The photo-electric effect thus produces in the electron energy spectrum a mono-energetic peak [6]). The photo-electric effect makes a large contribution to the absorption when E_0 is smaller than 200 keV; the absorption of soft and moderately hard X-radiation is almost entirely due to this effect. In this case, then, $\sigma \approx \sigma_f$.

In the second of the three processes — the *Compton effect* — a γ-quantum collides with an electron to which it transfers only a part E_c of its energy. It then continues on its way in a different direction (scattering) with an energy $E' = E_0 - E_c$. For a given direction of electron and scattered gamma quantum, it is possible to calculate E_c and E' by treating the gamma quantum as a particle having a kinetic energy E_0 (and E' after the collision) and a momentum E_0/c (or E'/c), and by applying to the collision process the laws of conservation of energy and momentum. The energy E_c transferred to the electron in this collision may have any value between 0 and $E_0/(1 + E_r/2E_0)$, where E_r is the energy corresponding to the rest mass of an electron, viz. 0.51 MeV. The spectrum of the E_c values is thus continuous, and the larger E_0 the larger the maximum value of E_c/E_0; at $E_0 = 2$ MeV this amounts to 0.80, and at 10 MeV to 0.977. The probability that a certain value of E_c will occur is a function of E_c and of E_0. With increasing E_0 the relatively small values of E_c decrease in significance and the energy spectrum of the Compton electrons acquires more the character of a peak.

---

[6]) In small crystals the X-ray quanta which "carry off" the binding energy E_b may nevertheless escape. In that case a residual "escape peak" is found beside the main photo-electric peak. If E_0 is of the order of 1 MeV or more, then $E_0 \gg E_b$ and the two peaks virtually coincide. This subject is dealt with at greater length on pp. 269-270 of the article quoted in [2]).

There is of course a chance that the scattered gamma quantum will be absorbed. If it is absorbed by the photo-electric effect, this again is a case of the entire energy E_0 being converted into electron kinetic energy; outwardly this is not to be distinguished from the direct occurrence of the photo-electric effect. Naturally, the chance of this happening increases according to the quantity of material used. With increasing scintillator size, therefore, the "photo-electric peak" becomes larger at the expense of the Compton continuum [7]).

The probability of a Compton collision, like the probability of photo-electric absorption, decreases with increasing E_0, but it does so in a much less pronounced way. In an NaI(Tl) crystal the probability of a Compton collision is already greater than that of the photo-electric effect at an E_0 value of 0.5 MeV.

The third process — *pair production* — occurs only when $E_0 \geqq 1.02$ MeV. The chance of this occurring increases with increasing E_0. Where E_0 is of the order of 10 MeV or more, pair production predominates over the other two effects. The process consists in the conversion of a gamma quantum into two particles which are identical except for their sign, namely an electron and a positon. The kinetic energy of the pair is $E_0 - 1.02$ MeV (i.e. E_0 less $2E_r$, the energy equivalent of the rest mass of the created particles). Thus, besides the "photo-peak" in the electron energy spectrum there may be a "pair peak", which is outwardly identical with the photo-peak caused by gamma quanta having an energy $E_0 - 1.02$ MeV. This pair peak is superimposed on the Compton continuum.

The average life of a positon is very short. It unites with an electron and the consequent annihilation of the pair gives rise to the emission of two identical but oppositely directed (conservation of momentum) gamma quanta each having an energy of 0.51 MeV. Generally this annihilation occurs when the positon has lost its kinetic energy; sometimes, however, also when it is in motion.

Naturally there is a certain chance that one or both annihilation quanta will be absorbed in the scintillator. If both are absorbed, then the entire E_0 is again absorbed and the photo-peak becomes larger at the expense of the pair peak. The cases, however, where only one of the annihilation quanta is absorbed give the appearance of a third peak in the electron energy spectrum, its position being exactly midway between the photo-peak (corresponding to the absorption of E_0) and the pair peak (absorption of $E_0 - 1.02$ MeV). In the absorption of gamma quanta by pair production the photo-peak will thus be relatively larger when a scintillator of larger mass is used, just as was the case with the Compton effect.

Fig. 4 shows the variation with E_0 of σ_f, σ_c and σ_p, and of their sum σ, for NaI. *Fig. 5* shows the spectrum of the energies transferred to the electrons in the case of gamma quanta of equal energy (in this case 2 MeV).

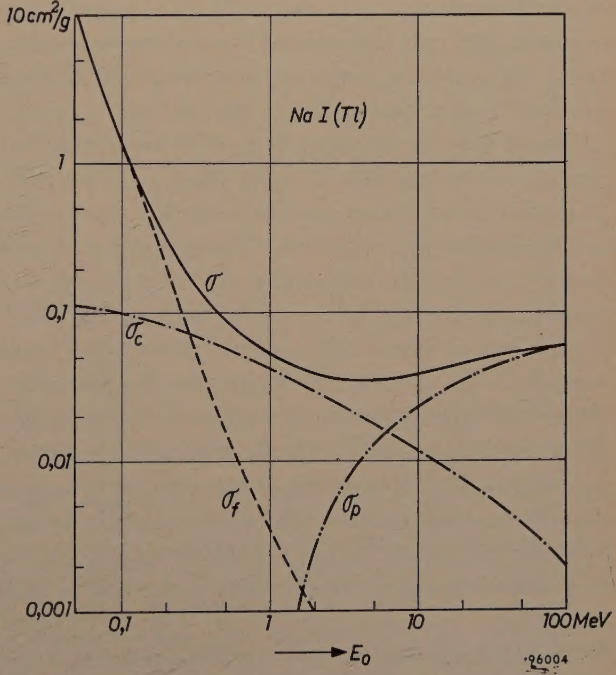

Fig. 4. Absorption of gamma radiation in NaI. The curves show how the contributions of the photo-electric effect (σ_f), the Compton effect (σ_c) and pair production (σ_p) to the mass attenuation coefficient (σ) depend on the quantum energy E_0.

---

[7]) The name "photo-electric peak" is really not applicable in this case; one should speak rather of a "peak of complete absorption".

The scintillation process

The energy E_1 which the liberated primary electrons have acquired from an incident gamma quantum is given up by these electrons in small amounts to other electrons in their path. After a short time the latter electrons have arrived at discrete energy levels above the ground state [8]. The subsequent events differ slightly from one scintillating material to another, but are essentially as follows. The "packet" of energy, corresponding to the difference in energy of an electron in the excited and in the ground state, is able to move through the scintillating material (i.e. it is transferred from electron to electron). At a certain moment, however, it is held up at some point, especially at places where foreign atoms or ions are situated (e.g. a Tl ion in the NaI crystal, or an impurity of some kind, or a molecule of dissolved substance), or in so-called *traps*, such as dislocations and vacancies. Upon capture in such a centre, a certain proportion of the energy is converted into thermal energy of the material. Depending on the nature of the centre, three things can happen to the remaining energy. In the first place it can be entirely or partly converted into a light quantum (fluorescence). The fluorescence light quanta emitted after absorption of one gamma quantum together constitute the light flash or scintillation. Secondly, de-excitation can take place via a radiationless transition (quenching). Thirdly the centre may possibly be one from which a lower energy level cannot be directly reached (trap). De-excitation may then occur by prior transition, owing to absorption of thermal energy, to a somewhat higher energy level (in the conduction band) from which a fluorescence centre can be reached (phosphorescence). Evidently, the material for a scintillation counter should exhibit a maximum of fluorescence and a minimum of quenching and of phosphorescence. The phosphorescence of NaI(Tl) and of plastic scintillators is low; in liquids it is entirely absent.

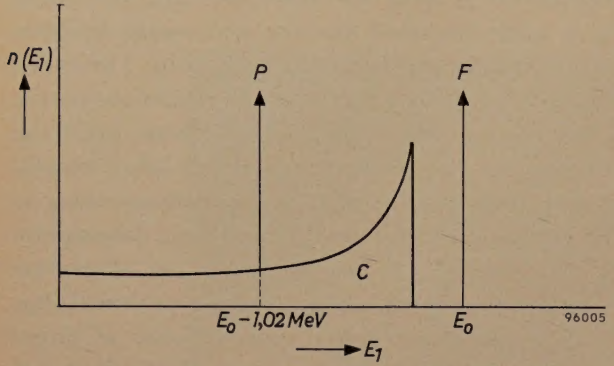

Fig. 5. Spectrum of the total energy E_1 of the primary electrons liberated by gamma quanta of 2 MeV. Note the Compton continuum (C), which is sharply cut off at the maximum Compton energy, and the "line" (F) of still higher energy. The latter is the "photo-electric peak", for which E_1 is equal to E_0, the energy of the detected gamma quanta. If, as in this case, the quantum energy is greater than 1.02 MeV, another "line", the pair peak (P), appears at a position corresponding to an energy $E_0 - 1.02$ MeV.

The number per unit time of the de-excitations by fluorescence is proportional to the number of occupied fluorescence levels (N) and to the number of unoccupied sites in the ground state. If the latter number is large compared with the first, so that it may be regarded as constant, we can write:

$$-\frac{\mathrm{d}N}{\mathrm{d}t} = \frac{N}{\tau_0}, \quad \ldots\ldots \quad (2)$$

where τ_0 is the average life of an electron in the energy state concerned and t the time. If N_0 is the value of N at $t = 0$, the solution of (2) is:

$$N = N_0\,\mathrm{e}^{-t/\tau_0}. \quad \ldots\ldots \quad (3)$$

The intensity of a scintillation accordingly decreases exponentially with time; the time constant is τ_0.

If the fluorescence light quanta have an average energy E_f — in NaI(Tl) about 3 eV — then the total energy of a single scintillation is N_0E_f. Owing to the quenching process and the radiationless transitions that occur together with the emission of light, this energy is smaller than the total absorbed energy E_1. The ratio η between E_1 and N_0E_f is called the *luminous efficiency* of the material. For NaI(Tl) the value of η is independent of E_1 and lies between 0.08 and 0.09.

From scintillation to electrical pulse; fluctuation phenomena

The N_0 light quanta that together form a scintillation will obviously not all strike the photocathode in the multiplier tube, nor does each quantum that *does* strike the photocathode produce an electron at the first dynode. The number of such electrons N_1 constitutes a fraction a of N_0. To produce a single effective photo-electron in the multiplier tube an energy E_i is therefore needed; this quantity, which we shall call the "*liberating energy*", is equal to $E_\mathrm{f}/a\eta$. Since a, like η, is about 0.08, the value of E_i is approximately 450 eV, i.e. about 15 times larger than in an ionization chamber or proportional counter. A gamma quantum of a given energy gives rise to larger pulses the larger is a, that is to say the smaller is E_i. The consequences of this will be discussed in the next section. The value of E_i for NaI(Tl) is independent of the energy of the incident gamma quantum.

---

[8] Many electrons initially receive more energy than they need to reach one of these levels; they then arrive in a higher continuum of energy levels, called the *conduction band*. While they remain in this band they can move through the crystal under the influence of an electric field. The action of the crystal counter (see [1]) is based on this phenomenon, which is more or less analogous to the ionization of a gas.

The value of a is greater the better the spectral sensitivity of the photocathode matches the spectrum of the scintillations. The dashed line in *fig. 6* represents the spectral energy distribution of scintillations from NaI(Tl). The maximum lies at about 4100 Å, i.e. well in the blue part of the spectrum. The solid curve represents the spectral sensitivity of Philips photomultiplier tube type 50 AVP, which is specially suited for mounting in scintillation counters and is used, for example, in the present equipment.

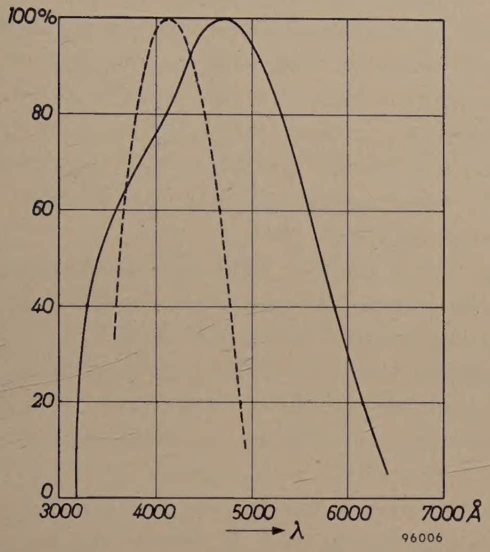

Fig. 6. Spectral intensity distribution of the scintillations in an NaI(Tl) crystal (dashed curve) and spectral sensitivity of the Philips photomultiplier tube 50 AVP. The maxima of both curves are given the value 100%.

When gamma quanta of a certain energy strike the scintillating crystal, the total energy E_1 of the electrons liberated by a single gamma quantum is not, as we have seen, of constant magnitude, but shows a complete spectrum of values (fig. 5). Even with constant E_1, however, certain fluctuations occur in the number of light quanta produced, in the fraction of this number that reaches the photocathode, in the number of photo-electrons liberated by a certain number of light quanta — i.e. in a and in η — and in the current gain g of the multiplier tube. One therefore measures at the output of the tube a spectrum of pulse amplitudes which may be regarded as a blurred version of the spectrum of electron energies E_1 (*fig. 7*).

The effect of these fluctuations is best demonstrated by the broadening of the photo-peak ($E_1 = E_0$). The position of this peak, i.e. the mean voltage of the pulses constituting the peak, is determined by the average values of a, η and g, and its width by the spread in these values.

The distribution of the values of N_1, the number of photo-electrons arriving at the first dynode per gamma quantum, can be described by a Gaussian distribution function, provided that $\bar{N}_1$, the mean value of N_1, is not too small. The standard deviation is equal to $\sqrt{\bar{N}_1}$. Frequently the half-height width of the Gaussian curve is taken, which is 2.36 × the standard deviation. The relative value of this measure of distribution is then $2.36/\sqrt{\bar{N}_1}$, and can also be written as $2.36\sqrt{E_0/E_i}$.

The variation of g which, together with the spread in N_1, determines the width of the photo-peak, can only be calculated subject to certain assumptions with regard to the secondary emission. We shall not deal with this here. Experiments have shown that the statistical fluctuations in g have relatively little effect on the blurring of the pulse spectrum.

The blurring of the pulse spectrum in consequence of the fluctuation phenomena described is principally of importance in scintillation spectrometry, which is touched on in the end of this article. It has no direct influence on the counting of the scintillations, and only rarely any indirect influence. In fact the high amplification in the multiplier tube allows pulses generated by a single photo-electron to appear above the noise of the pulse amplifier, even when g may happen to be particularly small.

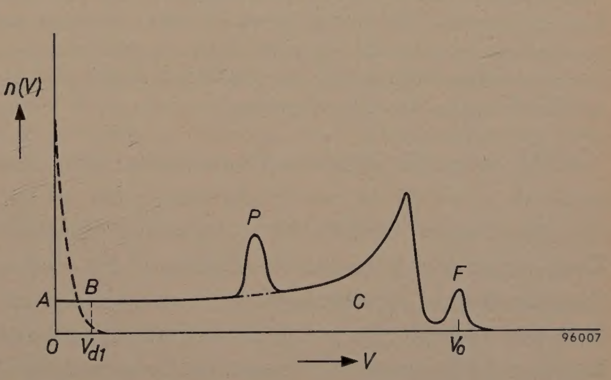

Fig. 7. Spectrum of the amplitude V of the electrical pulses delivered by the photomultiplier tube (solid curve). Owing to fluctuation phenomena in the scintillator and in the multiplier tube, the pulse-height spectrum does not exactly follow that of fig. 5, but is "blurred". The degree of blurring can be judged from the width of the peak F.

The dashed line gives the spectrum of the noise pulses; if the discriminator setting corresponds to a pulse-height V_{d1}, an average of one noise pulse per second is passed. This also suppresses a fraction of the wanted pulses equal to the ratio of the area $OABV_{d1}$ to the total area bounded by the solid curve. The ratio of the areas under the scintillation-pulse curve and the noise-pulse curve is here arbitrarily chosen. It depends on the noise intensity and the strength of the specimen under assay.

Counting the scintillations

Noise

Owing to the continuous energy spectrum of Compton electrons (as shown in fig. 7), there is a distinct possibility of small pulses occurring, even when the energy of the γ-quantum is large. From the conclusion of the last section it might be inferred that all these small pulses would be counted, down to about the voltage corresponding to the liberating energy E_i (about 450 eV). The actual situation, however, is somewhat less favourable owing to the inherent noise in the photomultiplier tube.

This noise is due to the fact that the photocathode emits a certain number of electrons per unit time even in the absence of incident light; these electrons give rise to spurious pulses (of the order of 10 000 per sec). The pulse-height distribution of this noise [9]) is represented by the dashed line in fig. 7. Most noise pulses originate from a single primary electron, only a small number from more than one.

The great majority of the noise pulses are due to the thermionic emission of electrons from the photocathode, which depends on the temperature and on the work function of the cathode material. It is a fortunate circumstance that many scintillating materials emit very strongly in the blue part of the spectrum, and it is therefore not necessary to select cathode materials having a very low work function. The noise pulses caused by thermionic emission all correspond, of course, to a single electron leaving the photocathode (mono-electronic pulses).

The relatively few poly-electronic pulses are presumably caused by residual gas ions colliding against the photocathode.

Two other causes of noise are thermionic and field emission from the dynodes. The first gives rise to pulses which, on an average, are much smaller than the above-mentioned mono-electronic pulses. Field emission can be virtually eliminated by suitably designing the dynode system.

If the enormous number of noise pulses were also counted, it would be practically impossible to use the scintillation counter as a radiation monitor. They can of course be largely eliminated by setting the pulse-height discriminator to a value V_{d1} such that, for example, only one noise pulse is counted per second. This naturally means that a certain fraction of the scintillation pulses will no longer be counted. This fraction can be found by dividing the area $OABV_{d1}$ in fig. 7 by the total area bounded by the curve representing the pulse spectrum. The fraction of uncounted pulses is smaller the larger is V_0 (see fig. 7) in relation to V_{d1}, or in other words, the smaller the liberating energy E_i. Further, a scintillator of larger dimensions is advantageous, in that relatively more gamma quanta then give rise to pulses in the photo-peak F of the spectrum than in the continuum C (fig. 5). The fulfilment of the first requirement, a small E_i value, depends on the following factors.

1) The number of light quanta produced in the scintillator by a colliding electron of a given energy, i.e. the luminous efficiency η. This is determined by the nature of the scintillating material.
2) The fraction of these light quanta that reaches the photocathode. If the scintillator is fully transparent, with one of its faces in good optical contact with the multiplier tube and with its other faces highly reflective, this fraction may closely approach 100%.
3) The chance of these light quanta liberating an electron from the photocathode. This chance, and the fraction mentioned under 2), together determine the value of the factor a introduced at the beginning of the last section.

In modern scintillation counters the undetectable fraction of the total number of scintillations amounts to only a few per cent. Other conditions being equal, the fraction is greater the lower the energy of the incident γ-quanta, for the value of V_0 is then smaller whereas the discriminator threshold is kept fixed at the value V_{d1} [10]).

To ascertain how the discriminator setting V_{d1} which leads to an average count of one noise pulse per second is related to V_0, it would be necessary to determine the value of V_0 and the form of the pulse spectrum. With the ordinary scintillation counting apparatus, however, this is not readily possible.

This object can nevertheless be achieved by plotting a curve of the counting rate versus the voltage (counting characteristic). Using a γ-active sample of constant intensity, the high tension H on the multiplier tube is varied while the discriminator setting V_d remains unchanged. Since the current amplification factor of the multiplier tube depends very closely on H, the variation of H implies a variation of V_0; with increasing H the value of V_0 increases, so that V_d/V_0 decreases. The pulse spectrum is extended but V_d remains constant. At all values of H where V_d is exceeded by a peak in the pulse spectrum (fig. 7), the number of pulses counted per unit time (the ordinate value of the curve) sharply increases.

---

[9]) By "noise" we refer to all unwanted pulses arising from random processes and which together constitute the "dark current". Spurious pulses associated with the scintillations are therefore not included under this term.

[10]) This relationship is not valid in all circumstances. If E_0 is small (< 100 keV) the continuum C (fig. 7) is of little significance compared with the peak F. This effect again reduces the undetectable fraction.

The numbers in *fig. 8* indicate the points of correspondence between the pulse-height spectrum and the counting characteristic, i.e. those abscissa values of the spectrum that are equal to V_d at the various H values. With increasing H the characteristic asymptotically approaches the maximum value (points *7* to *11*), but as soon as V_d is made smaller than V_{d1} (the discriminator threshold at which, for a given H, one noise pulse per second is counted), more and more noise pulses start to be counted and the total count rate again rises sharply with H.

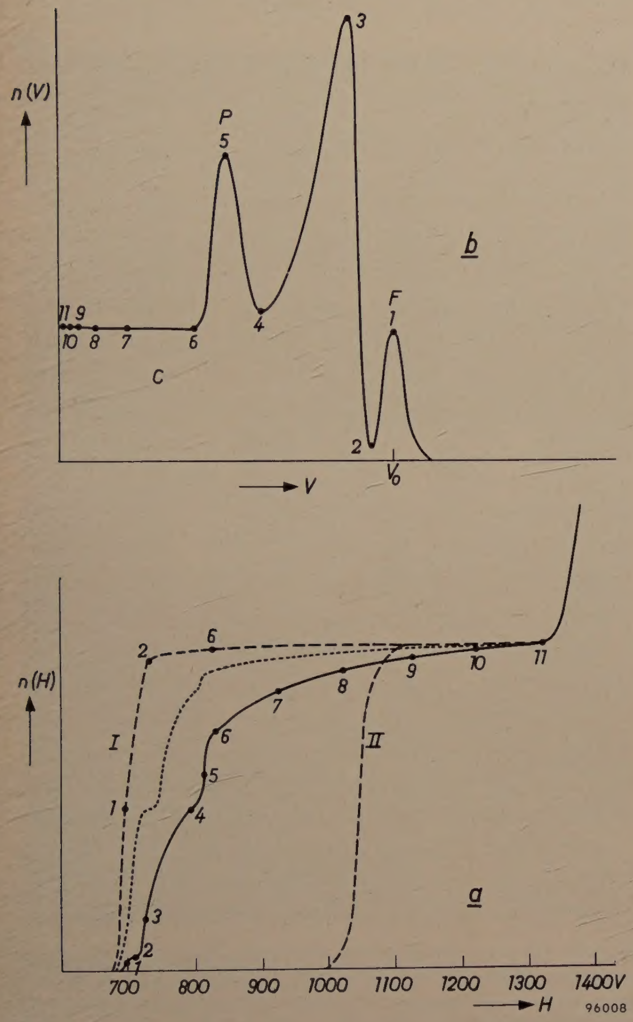

Fig. 8. The counting characteristic (a) of a scintillation counter is obtained by varying the voltage H on the photomultiplier tube while keeping the discriminator setting constant. Since the current gain of this tube varies with H (roughly in proportion with the 8th to 10th power of H), the result obtained in this way resembles that which would be obtained by keeping H constant and varying the discriminator setting V_d from the maximum pulse-height to 0. When V_d is exceeded by a peak in the pulse-height spectrum (b), the counting rate rises sharply. The numbers indicate the points of correspondence between the two curves. If V_0 is large with respect to V_d (points *7* to *11*), the number of counted pulses no longer varies markedly with H, but approaches the maximum value asymptotically. If H is very high (i.e. if V_0 is relatively *very* large with respect to V_d), more and more noise pulses are counted and the curve again rises steeply. The longer the horizontal part of the curve (the plateau), the better the counter. The solid curve applies to a small crystal, the dotted curve to a larger one and the dashed line *I* to an infinitely large crystal. Curve *II*, which has substantially the same form as curve *I*, applies to radiation of only 100 keV, the other curves to radiation of 2 MeV.

The substantially horizontal part of the counting characteristic is called the *plateau.*

The existence of this plateau — the region in which the count rate is substantially independent of H — naturally favours the accuracy of measurement. With a good-quality scintillation counter, i.e. one in which $V_{d1} \ll V_0$, the plateau is broad, whereas with a poor-quality counter it is narrow, or even absent (i.e. the two steep parts of the curve run immediately one into the other). On the other hand, it should not be forgotten that the shape of the characteristic and the length of the plateau also depend on the energy of the counted γ-quanta (see fig. 8), just as the ratio V_{d1}/V_0 does.

If we know the relation between the maximum pulse-height V_0 and the energy E_0 of the incident γ-quanta, we can calculate directly the equivalent γ energy to which V_{d1} corresponds. In modern scintillation counters this energy (E_{eq}) is 5 to 15 keV. In practice, E_0 varies from 50 to 3000 keV.

Since the ratio E_{eq}/E_0 is directly related to V_{d1}/V_0, the value of E_{eq} can also be regarded as a measure of the quality of the scintillation counter; the smaller is E_{eq}, the more favourable are the noise characteristics. For NaI(Tl), where V_0 is proportional to E_0, the ratios V_{d1}/V_0 and E_{eq}/E_0 are in fact identical, and E_{eq} is proportional to the liberating energy E_i.

The great advantage of secondary-emission amplification, as takes place in the photomultiplier tube, becomes evident if the multiplier tube in the scintillation counter is replaced by an ordinary photo-electric cell with amplifier. The minimum energy which the γ-quanta must then have in order to be counted amounts to several MeV. Pulses originating from quanta of less energy are drowned in the noise of the amplifier.

Other sources of noise in the equipment

Owing to the use of caesium in the fabrication of the multiplier tube (for the photocathode and sometimes also for the dynodes), the tube contains a small amount of caesium vapour. The caesium atoms may be ionized by colliding with electrons, and then move in the electrical field to the cathode. A pulse may therefore be followed a few µsec later (the transit time of the ions) by an "after pulse" [11]. When the voltage on the multiplier tube is high, this effect is by no means negligible and calls for an increase in the discriminator setting.

---

[11] See C. F. Hendee and W. B. Brown, Philips tech. Rev. **19**, 50-58, 1957/58.

Unwanted pulses are also caused by electrons exciting the anode into luminescence. The light so produced falls on the cathode and gives rise to undesired photo-emission. This effect also increases sharply with the tube voltage and, together with the above after-pulsing effect, determines the maximum permissible value of this voltage.

Background radiation

Whereas the noise pulses originating in the equipment itself can be adequately reduced in number by suitable pulse-height discrimination, tube voltage, etc., this is not the case as regards stray radiation. An ever-present source of such background is cosmic radiation, but natural radioactive substances in the surroundings and radioactive impurities in the counter itself also contribute to the background count.

The number of such quanta and particles incident on the scintillator can be limited by shielding the probe and the radioactive specimen inside a thick-walled lead "castle" (see fig. 3). For a probe containing an NaI(Tl) crystal of some tens of grammes, the background count can be reduced in this way from some scores to as few as 5 pulses per second. This method cannot, of course, be used in measurements on a patient, but an improvement is nevertheless possible with the aid of a lead collimator. This is a cylindrical or conical tube mounted in such a way that the scintillator "sees" only the part or organ of the body under investigation (*fig. 9*). If the background quanta are mainly of lower energy than the quanta to be counted, they can be entirely or largely suppressed by the discriminator. This admittedly reduces the counted fraction of the quanta to be counted, but this may not prove a serious drawback.

However this may be, it is necessary before carrying out any measurement to determine separately the number of background quanta occurring per unit time, and this should be done in conditions closely approaching those under which the measurement is performed. The true intensity of the radiation source is then subsequently found by deducting this background counting rate from the total counting rate.

Accuracy of measurement

Since the emission of radiation quanta or particles by radioactive atomic nuclei is a random phenomenon, the number of pulses (n) counted in a given time shows statistical fluctuations. The root mean square value of the fluctuations (standard deviation) is $\sqrt{\bar{n}}$ where $\bar{n}$ is the average value that would be found for n if the measurement were to be repeated a very large number of times. Two measurements on different specimens thus have the same relative error when they relate to the same number of quanta. To obtain the same relative precision, it is therefore necessary to make a measurement of longer duration on a weakly radioactive specimen than on a strongly radioactive specimen. With the Philips apparatus (fig. 3), this is done automatically, as already described. The "counting strategy" used, however, depends on the nature of the problem.

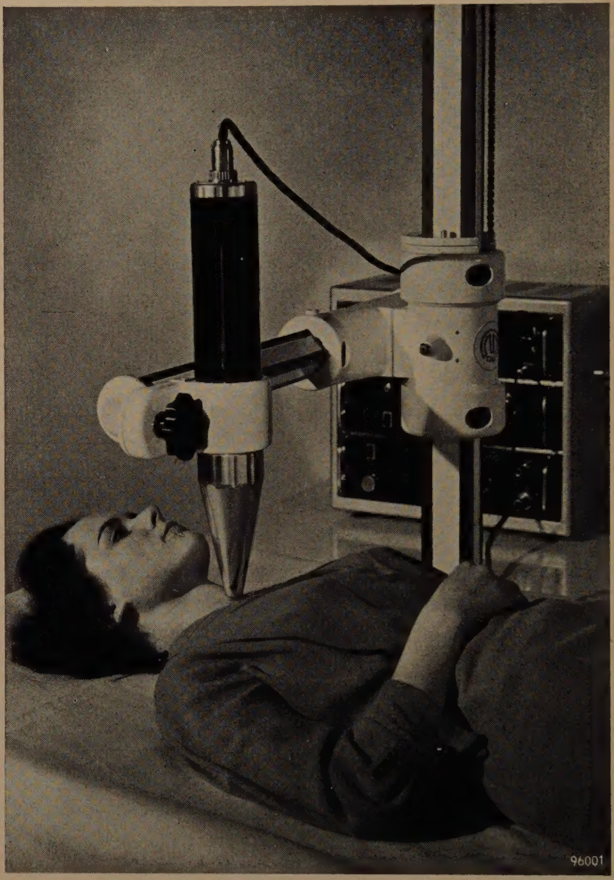

Fig. 9. In order to shield the scintillator from background radiation, the probe may be fitted in a lead collimator. With a very narrow collimator it is possible to chart the shape of an organ in which a radioactive substance has accumulated (see e.g. J. A. W. van der Does de Bye, Nucleonics 14, No. 11, 128-134, 1956). The photograph shows the set-up for a thyroid-gland examination.

For a treatment of these problems, which are by no means restricted to the scintillation method, the reader is referred to the article mentioned in footnote [5]).

Other scintillating materials and the detection of other radiations

In the foregoing we have been concerned in particular with the detection of γ radiation by a scintillation counter containing an NaI(Tl) crystal as scintillating material. For some measurements, NaI(Tl) has the drawback of a fairly long fluorescence decay constant (0.25 μsec). In some solid, monomer organic crystals the duration of a flash is a factor of 10 smaller (anthracene 3×10^{-8} sec), and is shorter still in plastic scintillators and certain scintillating fluids ($3\text{-}8 \times 10^{-9}$ sec).

The fluorescence decay constant of the latter substances approaches the spread in the transit time of the electrons in the multiplier tube. For the tubes which are best in this respect the spread is about 1.5×10^{-9} sec (on a transit time of 3×10^{-8} sec). When such "fast" materials are used, this spread partly determines the maximum counting rate, which represents the utmost limit of detection. Obviously, high demands are then made on the response of the associated electronic equipment.

Since α-particles have an extremely short range in a solid (some tens of microns), they can be detected with very thin layers of scintillating material, for example ZnS (activated by Ag) in powdered form. Moreover, since they are as a rule particles of very high energy, no trouble is experienced from unwanted radiation in measurements on an α-radiator. Compared with the detection of β and γ radiations, however, or with neutron detection, discussed below, the monitoring of α radiation is of less frequent occurrence. An example of its application will be found in article [3]).

Like γ-quanta, neutrons cannot be detected directly. Fast neutrons betray their existence by collisions with atomic nuclei, to which they give up part of their energy. The part given up is greater the lighter the excited nucleus, and hence is greatest for the hydrogen nucleus (proton). In this case the spectrum of the energy of collision runs from 0 to the full energy of the neutron (neutrons and protons having approximately the same mass) and has a sharp cut-off at these lower and upper values. Suitable scintillators are therefore organic substances, which are rich in hydrogen. A detectable fraction of neutron collisions, however, calls for a very large mass of material.

Thermal neutrons, which have an energy of about 0.025 eV, can only be detected via a nuclear reaction. For this purpose, lithium or boron is added to the scintillator; after capturing a thermal neutron, these atoms then emit a high-energy α-particle. Use is also made of single crystals of LiI(Sn) or LiI(Eu), but the latter are even more hygroscopic than NaI(Tl). Nuclear reactions in which only hard γ-quanta are emitted (which readily escape from the scintillator), or on which the daughter atoms (which remain in the scintillator) are radioactive, cannot of course be used.

Scintillation spectrometry

The fact that the height of the scintillation pulses varies with the absorbed gamma energy — and is proportional thereto in the case of NaI(Tl) — makes it possible with suitably calibrated apparatus to find the value of E_0 from the recorded pulse-heights. What is of special interest is V_0, the average pulse-height in the photo-peak; in this case the Compton continuum plays no part. Where we are concerned not with monochromatic gamma radiation but with the analysis of a gamma-ray *spectrum,* the presence of the Compton continuum is in fact a hindrance [12]). At high quantum energies, where the photo-peak is relatively small, the pair peak — which is then large — can be helpful, the average pulse-height in that peak being a measure of E_0 — 1.02 MeV.

Since a pulse spectrum is to be recorded, measures are needed to ensure that the measurement is not distorted by large pulses being clipped in the amplifier. The amplification should not be too high: it should be adjusted such that the discriminator threshold (1 noise pulse per sec) lies well below the linearity limit of the amplifier. When the usual type of pulse-height discriminator is used, the spectrum is presented in the form of an integrated pulse-height distribution from which the spectrum must then be derived by differentiation. A pulse-height spectrum can be obtained directly by using a differential discriminator, an instrument designed to pass only those pulses whose amplitudes lie within two close limits. In this way the analysis also gains in accuracy.

Variants of the normal scintillation spectrometer are the Compton and the pair spectrometer. The first of these uses two scintillation probes, which are set up a certain distance apart; coincidences are counted between pulses from the one probe, which is irradiated by the specimen, and pulses from the other, which is subjected solely to scattered gamma quanta with a specific scattering angle. The set-up is such that the γ-quanta measured are those scattered at some angle greater than 90°, for in this region the energy spectrum of the colliding electrons is fairly narrow, making it possible to calculate E_0 with reasonable accuracy from the known scattering angle and the energy transferred to an electron.

The pair spectrometer uses three probes, set up such that the three scintillators lie on a straight line. The middle probe is irradiated and the other two detect annihilation quanta. The pulses are counted in three-fold coincidence and the amplitudes of the pulses from the middle probe are measured. From the "normal" pulse spectrum, then, only the pair peak is selected for each component of the investigated radiation.

The energy resolution of a spectrometer, i.e. the ability to distinguish between γ-quanta of slightly different energy, is naturally better the narrower the photo-electric or pair peak. Here, too, a small value of E_i is desirable.

Summary. As opposed to other instruments for detecting radiations from radioactive substances, the scintillation counter is based not on the accumulation of electrical charges produced by ionizing events, but on the fact that in certain substances a short-lived flash of light (scintillation) occurs upon excitation. The scintillation is detected by means of a photomultiplier tube. Provided the scintillating material is optically transparent, its size can be increased without unduly impairing the detectability of the scintillations. A large detector can therefore be used, consisting of a substance of high density; this results in a satisfactory quantum counting efficiency even for hard gamma rays.

In the Philips scintillation counter, discussed in this article, the pulses delivered by the multiplier tube are passed, via an amplifier and a pulse-height discriminator, to a decade scaling circuit. The pulses vary in amplitude between zero and a maximum value corresponding to the total energy of the gamma quantum. The form of the pulse-height spectrum is determined by the three processes involved in the absorption of gamma quanta, viz. the photoelectric effect, the Compton effect and pair production. The excitation to which this absorption gives rise in the scintillating crystal leads to instantaneous or delayed light emission (fluorescence and phosphorescence) and also to radiationless transitions. In some scintillators, including the widely used NaI(Tl) crystal, the pulse-height is proportional to the absorbed energy. However, since the excitation-scintillation process and the chance of a light quantum striking the photocathode are subject, like the response of the multiplier tube, to fluctuations, the pulse-height spectrum is only a "blurred" version of the true absorption spectrum. In the range of low-amplitude pulses, moreover, detection is hampered by noise pulses originating from the multiplier tube. These can be largely suppressed by an appropriate setting of the discriminator, without which it would be impossible to monitor weakly radioactive specimens. In modern counters this setting corresponds to the maximum height of pulses arising from gamma quanta of 5 to 15 keV.

The counting system in the Philips apparatus is designed to allow the counting rate to be determined either from the number of pulses recorded in a given time or from the time interval taken to accumulate a predetermined number of counts. To suppress background radiation during a measurement, the specimen and the "probe" — which contains the scintillator, the photomultiplier tube and a cathode-follower pre-amplifier valve — are placed in a lead "castle". When the nature of the measurement precludes this form of shielding, a lead collimator may be used. With a very narrow collimator it is possible to chart the shape of a radioactive object (e.g. the thyroid gland of a patient to whom ^{131}I has been administered).

---

[12]) The gamma-ray spectra of radioactive substances possess roughly 1 to 10 spectral lines. Although this number is small compared with the number of lines usually found in optical spectra, the analysis of a spectrum with 10 lines, particularly when some of them are weak, imposes heavy demands on a scintillation spectrometer.

A METHOD OF MEASURING THE RESISTIVITY AND HALL COEFFICIENT ON LAMELLAE OF ARBITRARY SHAPE

621.317.331:538.632.083

Resistivity and Hall-coefficient measurements at different temperatures play an important part in research on semiconductors, such as germanium and silicon [1], for it is from these quantities that the mobility and concentration of the charge carriers are found.

Such measurements are commonly carried out with a test bar as illustrated in *fig. 1*. The resistivity is found directly from the potential difference and the distance between the contacts O and P, the current i and the dimensions of the bar. To determine the Hall coefficient the bar is subjected to a magnetic field B applied at right angles to the direction of the current and to the line connecting the diametrically opposite contacts O and Q. From the potential difference thus produced between these latter contacts the Hall coefficient is derived. (The relation between the Hall coefficient and the change in electric potential distribution due to a magnetic field will be explained presently.)

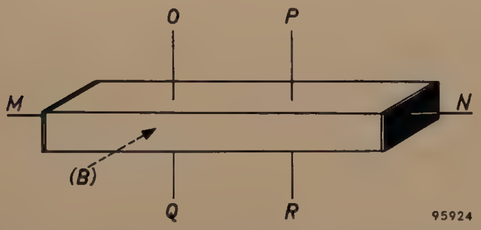

Fig. 1. Classical form of sample used for resistivity and Hall-coefficient measurements. The test bar is provided with current contacts M and N and voltage contacts O, P, Q and R. The fourth voltage contact R serves for check measurements.

In measurements performed at low temperatures — e.g. in liquid nitrogen — point contacts possess resistances of the order of megohms, in consequence of which the voltages cannot be determined with sufficient accuracy. In such cases "bridge-shaped" samples are used as illustrated in *fig. 2*. The voltage and current contacts here have a relatively large surface area, and hence the contact resistances are low.

The methods referred to are based on the fact that the geometry of the sample ensures a simple pattern of virtually parallel current stream-lines. Formulae have been devised to correct for the deviation from parallelism in fig. 2, caused by the finite width of the arms. A drawback of the bridge-shaped sample is that it is rather difficult to make, having to be cut out of the brittle semiconductor material with an ultrasonic tool. There is therefore a considerable risk of breakage, particularly when the arms are made narrow.

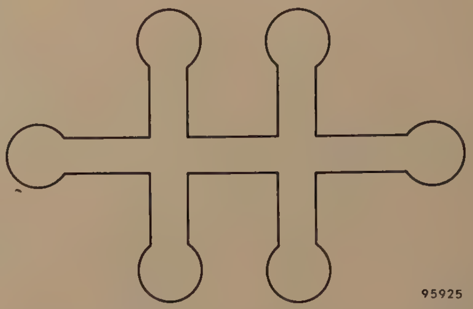

Fig. 2. The bridge-type sample, which is provided with relatively large contact faces to reduce contact resistances. This form is of special importance in measurements at low temperatures.

In the following we shall describe a method of performing resistivity and Hall-coefficient measurements on lamellae of arbitrary shape [2]. The lamella must not, however, contain any (geometrical) holes.

New method of measuring resistivity

We take a flat lamella, completely *free of holes*, and provide it with four *small* contacts, M, N, O and P, at arbitrary places *on the periphery* (*fig. 3*). We apply a current i_{MN} to contact M and take it off at contact N. We measure the potential difference $V_P - V_O$ and define:

$$R_{MN,OP} = \frac{V_P - V_O}{i_{MN}}.$$

Analogously we define:

$$R_{NO,PM} = \frac{V_M - V_P}{i_{NO}}.$$

The new method of measurement is based on the theorem that between $R_{MN,OP}$ and $R_{NO,PM}$ there exists the simple relation:

$$\exp\left(-\frac{\pi d}{\varrho} R_{MN,OP}\right) + \exp\left(-\frac{\pi d}{\varrho} R_{NO,PM}\right) = 1, \quad (1)$$

where d is the thickness of the lamella and ϱ the resistivity of the material. If d and the "resistances" $R_{MN,OP}$ and $R_{NO,PM}$ are known, then (1) yields an equation in which ϱ is the only unknown quantity.

---

[1] See e.g. C. Kittel, Introduction to solid state physics, 2nd edition, Wiley, New York 1956, Chapter 13, p. 347 et seq.

[2] L. J. van der Pauw, A method of measuring specific resistivity and Hall effect of discs of arbitrary shape, Philips Res. Repts. **13**, 1-9, 1958 (No. 1).

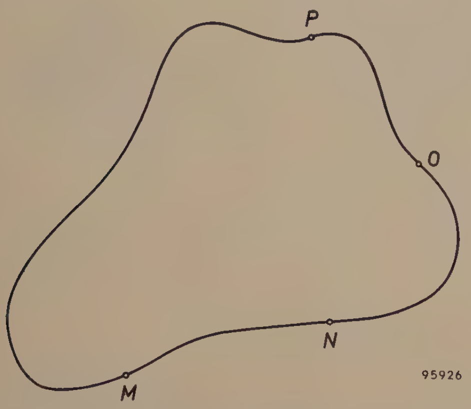

Fig. 3. A flat lamella of arbitrary shape, with four contacts *M*, *N*, *O* and *P* on the periphery, as used in the new method of measuring resistivity. The Hall coefficient can also be measured on a sample of this kind.

The situation is particularly straightforward if the sample possesses a line of symmetry. In that case, *M* and *O* are placed on the line of symmetry, while *N* and *P* are disposed symmetrically with respect to this line (*fig. 4*). Then:

$$R_{NO,PM} = R_{MN,OP}, \quad . \; . \; . \; . \; . \quad (2)$$

which may be seen as follows. From the reciprocity theorem for passive fourpoles, we have quite generally that $R_{NO,PM} = R_{PM,NO}$ (interchange of current and voltage contacts), and it follows from the symmetry that $R_{PM,NO} = R_{MN,OP}$. Hence we arrive at (2); ϱ can then easily be found from (1):

$$\varrho = \frac{\pi d}{\ln 2} R_{MN,OP}. \quad . \; . \; . \; . \; . \; . \; . \quad (3)$$

In this case a single measurement suffices.

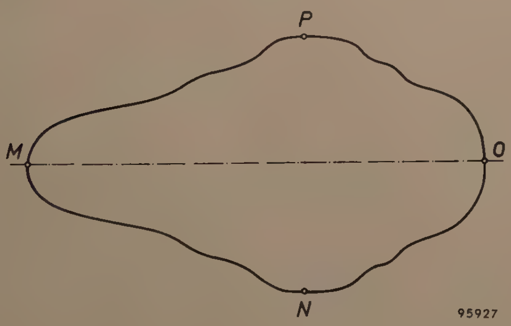

Fig. 4. The resistivity measurement is simplified if the sample has a line of symmetry. If two of the contacts are situated on the line of symmetry and the two others are symmetrically situated with respect to this line, one measurement is sufficient to give the required resistivity.

In the general case it is not possible to express ϱ explicitly in known functions. The solution can, however, be written in the form

$$\varrho = \frac{\pi d}{\ln 2} \frac{R_{MN,OP} + R_{NO,PM}}{2} f, \quad . \; . \; . \quad (4)$$

where f is a factor which is a function only of the ratio $R_{MN,OP}/R_{NO,PM}$, as plotted in *fig. 5*. Thus, to determine ϱ, we first calculate $R_{MN,OP}/R_{NO,PM}$, read from fig. 5 the corresponding value of f and then find ϱ from (4).

Photographs of samples as used for the old and for the new method are shown in *fig. 6*.

The complete proof of the theorem underlying the measurement of ϱ is given in the paper quoted in footnote ²). The proof consists of two parts. First of all, relation (1) is developed for a special case, the case of a lamella in the form of an infinite half-plane, provided with four contacts at the periphery. It is then shown that the relation must also apply to a lamella of any shape. This is done by means of conformal mapping of the arbitrarily shaped plate on the infinite half-plane with the aid of complex functions.

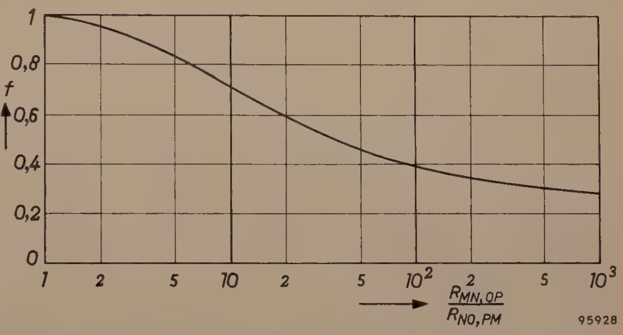

Fig. 5. Between the factor f in formula (4) and the ratio $R_{MN,OP}/R_{NO,PM}$ there exists the relation:

$$\cosh\left\{\frac{(R_{MN,OP}/R_{NO,PM})-1}{(R_{MN,OP}/R_{NO,PM})+1}\,\frac{\ln 2}{f}\right\} = \tfrac{1}{2}\exp\frac{\ln 2}{f},$$

which is represented here graphically.

We shall consider the first part of the proof in more detail, since it reveals the origin of the exponential functions in (1).

We first consider a lamella which extends to infinity in all directions. To a point *M* we apply a current $2i$, which flows away from *M* with radial symmetry into infinity. Let d again be the thickness of the lamella and ϱ the resistivity. Then at a distance r from *M* the current density is

$$J = 2i/2\pi r d.$$

The field-strength E is radially oriented and according to the generalized form of Ohm's law has the value:

$$E = \varrho J = \varrho i/\pi r d.$$

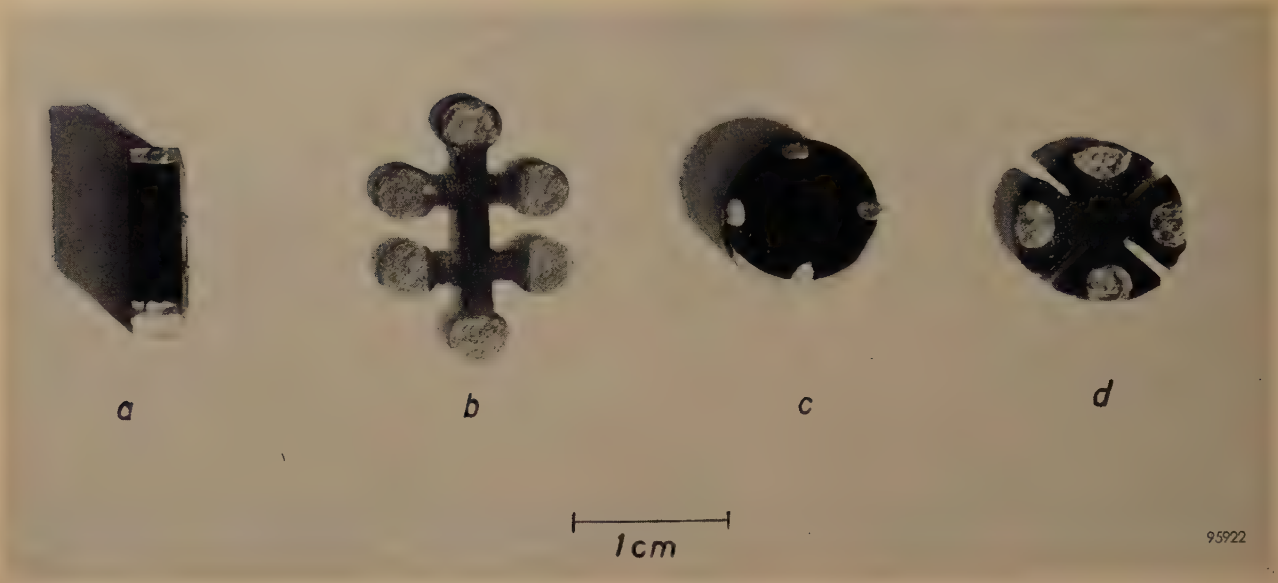

Fig. 6. Some samples of silicon used for resistivity and Hall-coefficient measurements. Samples *a* and *b* correspond respectively to figs. 1 and 2. Measurements on samples *c* and *d* are possible only by the new method. The incisions in sample *d* serve to reduce the error caused by the contacts not being infinitely small.

The potential difference between two points *O* and *P* lying on a straight line with *M* (*fig. 7a*) is:

$$V_P - V_O = \int_P^O E\,\mathrm{d}r = \frac{\varrho i}{\pi d}\int_P^O \frac{\mathrm{d}r}{r} = -\frac{\varrho i}{\pi d}\ln\frac{a+b+c}{a+b}.$$

Since no current flows in the direction perpendicular to the line through *M*, *O* and *P*, the result obtained remains valid if we omit the part of the lamella at one side of this line — yielding a half-plane — and if at the same time we halve the current (fig. 7*b*).

Next we consider the case of *c*) in fig. 7, where a current *i* now flows *out* from a point *N*, that again lies on the same straight line with *OP*, viz. on the edge of the infinite half-plane. We now find:

$$V_P - V_O = +\frac{\varrho i}{\pi d}\ln\frac{b+c}{b}.$$

Superposition of the cases *b*) and *c*) in fig. 7 yields the case *d*), the current *i* being introduced at *M* and taken off at *N*. The value now assumed by $V_P - V_O$ is found by adding together the two previous results. After dividing by *i* we then find:

$$R_{MN,OP} = \frac{\varrho}{\pi d}\ln\frac{(a+b)\,(b+c)}{(a+b+c)b},$$

or

$$\frac{(a+b+c)b}{(a+b)\,(b+c)} = \exp\left(-\frac{\pi d}{\varrho}\,R_{MN,OP}\right).$$

Similarly we find:

$$\frac{a\,c}{(a+b)\,(b+c)} = \exp\left(-\frac{\pi d}{\varrho}\,R_{NO,PM}\right).$$

Addition of the last two equations yields (1).

We shall now explain how formula (4) follows from (1). For simplification we put:

$$\left.\begin{aligned}\pi\,d\,R_{MN,OP} &= x_1,\\ \pi\,d\,R_{NO,PM} &= x_2.\end{aligned}\right\} \quad \ldots\ldots\ldots \quad (5)$$

Formula (1) can then be written:

$$\mathrm{e}^{-\frac{x_1}{\varrho}} + \mathrm{e}^{-\frac{x_2}{\varrho}} = 1. \quad \ldots\ldots\ldots \quad (6)$$

Next we write:

$$x_1 = \tfrac{1}{2}\{(x_1+x_2)+(x_1-x_2)\}$$

$$\text{and}\quad x_2 = \tfrac{1}{2}\{(x_1+x_2)-(x_1-x_2)\},$$

whereby (6) takes the form:

$$\mathrm{e}^{-\frac{x_1+x_2}{2\varrho}}\left(\mathrm{e}^{-\frac{x_1-x_2}{2\varrho}} + \mathrm{e}^{+\frac{x_1-x_2}{2\varrho}}\right) = 1.$$

This is the same as:

$$\mathrm{e}^{-\frac{x_1+x_2}{2\varrho}}\cosh\frac{x_1-x_2}{2\varrho} = \tfrac{1}{2}. \quad \ldots\ldots \quad (7)$$

The exponent of e in (7) is now written as —(ln 2)/*f*, i.e. we put:

$$\frac{x_1+x_2}{2\varrho} = \frac{\ln 2}{f}. \quad \ldots\ldots\ldots \quad (8)$$

Formula (7) then becomes:

$$\mathrm{e}^{-\frac{\ln 2}{f}}\cosh\left\{\frac{(x_1/x_2)-1}{(x_1/x_2)+1}\times\frac{\ln 2}{f}\right\} = \tfrac{1}{2}.$$

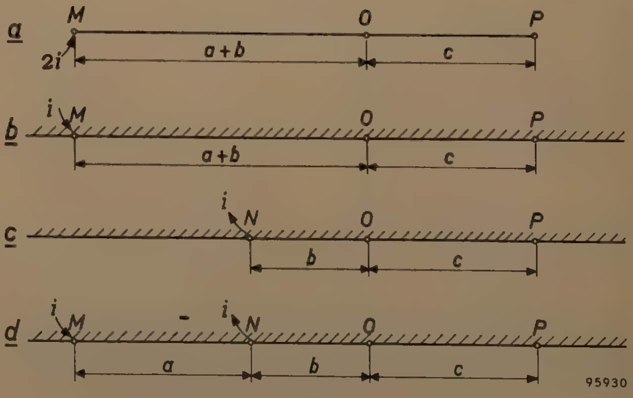

Fig. 7. Illustrating the derivation of formula (1).

This expression represents a relation between f and x_1/x_2, and hence also between f and $R_{MN,OP}/R_{NO,PM}$ (see 5). The relation is shown graphically in fig. 5. By re-writing (8) to give ϱ and substituting for x_1 and x_2 from (5), we find formula (4).

Method of measuring the Hall coefficient

The Hall coefficient, too, can be measured on an arbitrary lamella as in fig. 3. We then apply the current to one of the contacts, say M, and take it off at the contact following the succeeding one, i.e. in our case at O. We measure $R_{MO,NP}$, after which we set up an uniform magnetic induction B at right angles to the surface of the lamella. This changes $R_{MO,NP}$ by an amount $\Delta R_{MO,NP}$. We shall now denote the Hall coefficient R_H and show that it is given by:

$$R_H = \frac{d}{B} \Delta R_{MO,NP}, \quad . \ . \ . \ . \quad (9)$$

provided that:

a) the contacts are sufficiently small,

b) the contacts are on the periphery,

c) the lamella is of uniform thickness and free of holes.

The validity of formula (9) depends on the distribution of current stream-lines not changing when the magnetic field is applied. With samples of the classical shape of figs. 1 and 2, where the current stream-lines are always parallel to the edges of the sample, there is evidently no change. From the properties of the vector field representing the current density it follows that the same also applies to lamellae of arbitrary shape, provided the above conditions are satisfied [3].

Under the magnetic induction B, the charge carriers, with charge q, are subjected to a force perpendicular to the stream-lines and perpendicular to the lines of magnetic induction. The magnitude of this force is $F = qvB$, where v is the velocity of the charge carriers. Between v, the concentration n of the charge carriers and the current density J there exists the relation $v = J/nq$. Dividing the force exerted on the charge carriers by their charge q, we see that the effect of the magnetic field is equivalent to an apparent electric field E_H, the Hall electric field, for which we can write [4]:

$$E_H = \frac{1}{nq} J B .$$

E_H is proportional to J and to B; the proportionality constant ($= 1/nq$) is called the Hall coefficient R_H.

Since q is known, one can calculate from R_H the concentration n of the charge carriers.

The fact that the current stream-lines are not affected by the magnetic field implies that after application of the magnetic field the electric field is no longer in the same direction as the current stream-lines, but has acquired a transverse component E_t which exactly compensates the apparent Hall electric field E_H (*fig. 8*). The change $\Delta(V_P - V_N)$ in the potential difference between P and N is therefore given by integrating E_t from P over a path orthogonal to the current stream-lines to N' across the lamella (*fig. 9*), and thence along the periphery — i.e. along a stream-line — from N' to N. The last portion of the path makes no contribution to the integral; hence

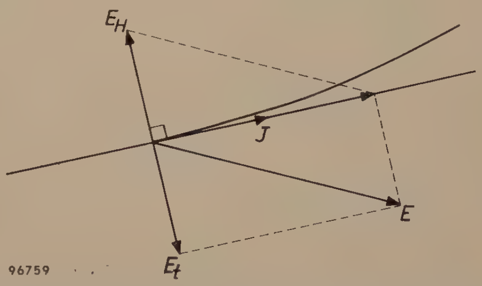

Fig. 8. The resultant of the electrical field-strength E and the Hall field-strength E_H lies in the direction of the current density J. Resolving E in directions perpendicular and parallel to J therefore yields a perpendicular component E_t which in magnitude is equal to E_H.

$$\Delta(V_P - V_N) = \int_P^{N'} E_H \, ds = R_H B \int_P^{N'} J ds = R_H B \frac{i_{MO}}{d},$$

where d is again the thickness of the lamella. This expression leads directly to (9).

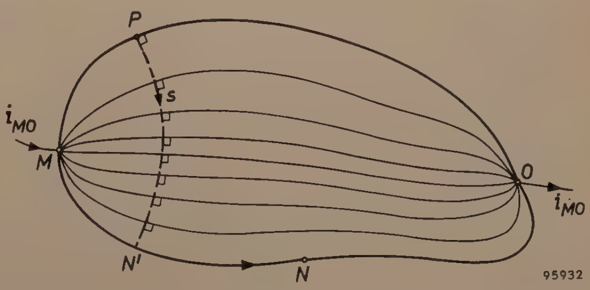

Fig. 9. To calculate by how much the potential difference between points P and N changes when a magnetic field is applied at right-angles to the plane of the sample, the transverse electric field E_t produced by the magnetic field is integrated along the path s which runs from P, orthogonal to the current stream-lines, to N' and thence along the periphery from N' to N.

---

[3] The proof of this statement is also indicated in the paper quoted under [2].

[4] This formula is not entirely exact because, apart from their ordered motion with velocity v, the electrons also move randomly owing to thermal agitation. More precise calculation shows, however, that the formula given here is a good approximation.

Estimation of errors

In the foregoing we have assumed the contacts to be "sufficiently" small and to be situated on the periphery. To gain an idea of the error made in the calculations when these conditions are not exactly satisfied, we have worked out the error for three cases. For simplicity we consider a circular disc of diameter D with the contacts mutually 90° apart. We assume further that only one of the contacts is not ideal. The three cases are represented in the adjoining *table*, together with the formulae for the relative errors in the resistivity and the Hall coefficient. The cases are:

a) One of the contacts has a length l along the periphery.

b) One of the contacts has a length l perpendicular to the periphery.

c) One of the contacts, although a point, is situated at a distance l from the periphery.

In practice, none of the contacts will be ideal. To the first approximation the total error is then equal to the sum of the errors per contact.

Table. The relative errors $\Delta\varrho/\varrho$ and $\Delta R_{\rm H}/R_{\rm H}$ in the calculated values of the resistivity and the Hall coefficient for a circular disc of diameter D on which one contact P is non-ideal, in the senses indicated in the sketches.

	$\Delta\varrho/\varrho$	$\Delta R_H/R_H$
a 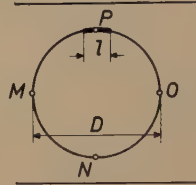	$\approx \dfrac{-l^2}{16D^2\ln 2}$	$\approx \dfrac{-2l}{\pi^2 D}$
b 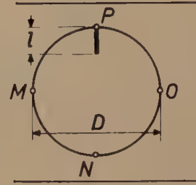	$\approx \dfrac{-l^2}{4D^2\ln 2}$	$\approx \dfrac{-4l}{\pi^2 D}$
c 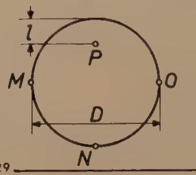	$\approx \dfrac{-l^2}{2D^2\ln 2}$	$\approx \dfrac{-2l}{\pi D}$

95929

The value of the method described here lies in the fact that, in many cases, the material under investigation is already available in the form of small lamellae (e.g. thin discs sawn from a crystal rod); these samples now need no further preparation and can therefore be used for other purposes after the measurement.

If very small contacts are undesirable, having regard to contact resistances in measurements at low temperature, use can be made of "clover-leaf" samples (see fig. 6*d*), the incisions in which substantially reduce the error due to the finite dimensions of the contacts. The clover-leaf sample thus replaces the bridge-type sample (fig. 6*b*) which is used for the same purpose in the classical method. The clover-leaf sample is easier to make than the bridge-type sample and is also less susceptible to breakage.

L. J. van der PAUW.

THE EC 59, A TRANSMITTING TRIODE WITH 10 W OUTPUT AT 4000 Mc/s

by V. V. SCHWAB *) and J. G. van WIJNGAARDEN.

621.385.3.029.64

The versatility of the triode valve stems largely from its wide frequency coverage. Moreover, it operates on low supply voltages and needs no electron-focusing devices. These advantages over microwave tubes of the klystron and travelling-wave type have led to the development of triodes for operation at increasingly higher frequencies. A triode has now been developed in the Philips laboratories which can be used very successfully as a transmitting tube in microwave radio links for relaying telephony and television signals on 7.5 cm waves. Its high power output ensures good communications even under conditions of strong interference.

Introduction

The type EC 59 transmitting triode is one of the most recent fruits of the development work on microwave triodes being carried out in the laboratories of the Philips concern. Following the completion of the disc-seal triodes EC 56 and 57 [1]), intended for operation at 4000 Mc/s, the need was felt for a tube which, at the same frequency, would be capable of delivering a power of 10 to 20 watts with reasonable power gain at a bandwidth of 100 Mc/s. During the relay of television programmes the hitherto available power output of 1.5 W, as delivered by the EC 57 triode, may, under adverse conditions (interference, fading), be too low to produce an acceptable signal-to-noise ratio at the receiving end. To allow for such contingencies, a certain surplus of transmitting power is desirable.

With the EC 59 triode, which is the subject of this article, it is now possible to meet these requirements. In a subsequent article a description will be given of the amplifier designed to operate with this tube.

Theoretical considerations

Fundamentally the EC 59 triode resembles in many respects type EC 57, which was earlier described in this Review. Both tubes are "disc-seal" triodes, characterized by the planar structure and rotational symmetry of their electrode systems.

In a triode the time τ_{kg} taken by an electron to reach the grid is determined by the distance travelled, d_{kg}, and by the mean potential V_0 in the grid plane:

$$\tau_{kg} = \frac{3\,d_{kg}}{\sqrt{2\,\dfrac{e}{m}\,V_0}} \quad . \; . \; . \; . \; . \; . \; . \; . \quad (1)$$

Here e and m are respectively the charge and mass of an electron. For the tube to function properly, this transit time should be small compared with the time T of one cycle of the input signal.

It might appear from (1) that by raising the potential V_0 one could arbitrarily shorten the transit time. According to Child's law [2]), however, the current density J of the emission of the cathode is also governed by V_0 and d_{kg}:

$$J = \frac{4}{9}\,\varepsilon_0 \sqrt{2\,\frac{e}{m}}\;\frac{V_0^{\frac{3}{2}}}{d_{kg}^{\;2}} \quad . \; . \; . \; . \quad (2)$$

(ε_0 = dielectric constant of vacuum), and the result of raising V_0 indefinitely would therefore be to saturate the cathode and so drive the tube beyond control. One can get a better idea of the possible ways of reducing τ_{kg} by eliminating V_0 from both equations. One then finds, with d_{kg} in cm and J in ampere/cm^2,

$$\tau_{kg} = 6.7\times 10^{-10} \left(\frac{d_{kg}}{J}\right)^{\frac{1}{3}} \text{sec.}$$

At 4000 Mc/s, then, where the period T is 2.5×10^{-10} sec, the relative transit time is:

$$\frac{\tau_{kg}}{T} = 2.68 \left(\frac{d_{kg}}{J}\right)^{\frac{1}{3}} . \; . \; . \; . \; . \; . \quad (3)$$

It can be seen that the relative transit time can be minimized by reducing the distance d_{kg} and also by increasing the current density J. Thus, where the grid-to-cathode distance is made larger in a given case, it is still possible to maintain the same transit time by increasing the current density.

---

*) Member of the Development Laboratory of Valvo G.m.b.H. Radioröhrenfabrik, Hamburg.

[1]) G. Diemer, K. Rodenhuis and J. G. van Wijngaarden, The EC 57, a disc-seal microwave triode with L cathode, Philips tech. Rev. **18**, 317-324, 1956/57.

[2]) C. D. Child, Phys. Rev. **32**, 492, 1911.

The cathode

In view of the evident advantage of a high current density, the EC 59, like the EC 57, is provided with an L (dispenser) cathode. This is capable of supplying continuously the full saturation current, about 5 A/cm², whereas with an oxide cathode in this type of tube only 300 mA/cm² could be obtained, i.e. only a few % of its saturation current. Moreover, since, with the L cathode, the cathode current need not be so very much smaller than the saturation current, the space-charge potential minimum is flattened and also lies nearer to the emitting surface (see the article cited under [1])). This reduces the loss caused by electrons which, being unable to pass the potential minimum, return to the cathode, and in the process absorb energy from the high-frequency electromagnetic field (total-emission damping). A further advantage of the L cathode is that it is better able to withstand "back heating", a phenomenon discussed later in this article (see section in small print, p. 228). Also, owing to the emitting surface being metallic, it can be made flat and smooth and is not formed by a layer of fairly high resistance as in the case of an oxide cathode.

Considerations concerning the grid-anode space

For a transmitting tube the product of the output power P and the bandwidth B is of primary importance. It is given by the formula [3]):

$$P \times B = \alpha J^2 d_{ga} \frac{C_{ga}}{C_{ga} + C_s} a^2, \quad . \; . \quad (4)$$

where d_{ga} is the distance between grid and anode, a the radius of the cathode and of the anode (supposed equal), C_{ga} the capacitance between grid and anode in the tube, and C_s the remaining stray capacitance in parallel with C_{ga}; α is a factor allowing for the transit-time effects, the feedback and the dielectric losses in the glass, but is not relevant to the present considerations.

The product of power gain G and bandwidth B, which was discussed in the article cited under [1]), may be written in the somewhat modified form:

$$G \times B = \beta \sigma d_{ga} \frac{C_{ga}}{C_{ga} + C_s}, \quad . \; . \; . \quad (5)$$

where σ is the transconductance per unit area of cathode surface (this quantity depends solely on d_{kg} and J); β has a significance similar to that of α in (4).

We see that (4) and (5) contain, respectively, the factors

$$d_{ga}\, a^2 \frac{C_{ga}}{C_{ga} + C_s} \quad \text{and} \quad d_{ga} \frac{C_{ga}}{C_{ga} + C_s},$$

both of which are of a geometric nature. The designer of a transmitting tube sets out to achieve a specific value of the product $P \times B$, so that in this case the first factor is of primary importance. It is found that for a transmitting tube the value of a must be greater than for a receiving tube.

In order to see how the design of the EC 59 is affected by the above considerations, it will be necessary to examine the exact nature of C_{ga} and C_s. In the frequency range in which the tube operates, the output circuit is formed by a resonant cavity having a localized narrower space, where the electric field is concentrated and which is the gap traversed by the electrons ("re-entrant" cavity); see *fig. 1*. The anode surface and the grid plane constitute part of this cavity. This is the essence of the electrode configuration in a disc-seal triode [4]). To a first approximation one can represent

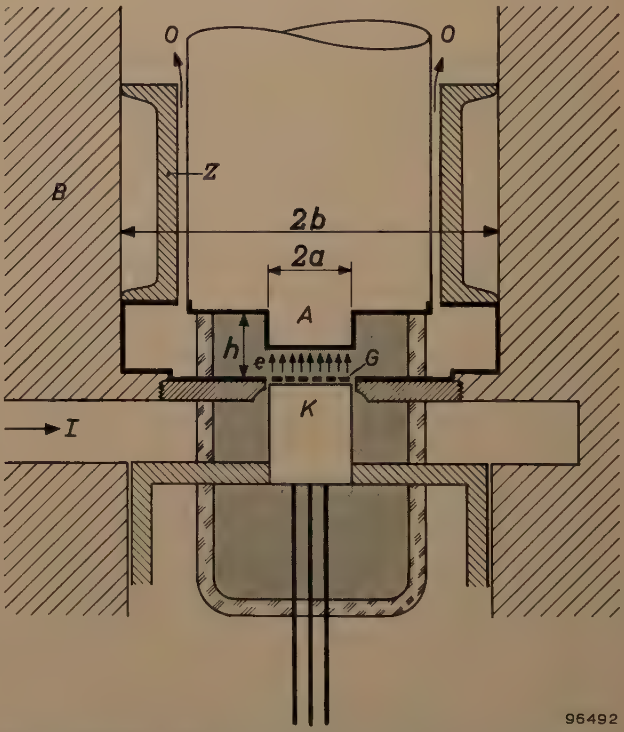

Fig. 1. Schematic diagram of a disc-seal triode, mounted in an amplifier, showing the output resonant cavity (bold lines). *A* anode, *G* grid, *K* cathode, *Z* tuning piston moving in metal block *B*. The glass spacer ring between grid and anode divides the resonant cavity into two parts, the inner part being evacuated (evacuated part of tube is shaded). The arrow *I* indicates the high-frequency energy entering via a waveguide, of which the very small cathode-grid gap forms a part. The small arrows *e* represent the electrons traversing the electrode space; the alternating electrical field of the resonant cavity is largely concentrated in this space. The two arrows *O* denote the high-frequency energy leaving the annular output gap (quarter-wave transformer).

---

[3]) J. G. van Wijngaarden, Onde électrique **36**, 888, 1956.

[4]) It is evident that the output circuit is not formed by the tube alone.

this resonant cavity electrically by a capacitance in parallel with a self-inductance. The capacitance consists partly of the capacitance between the two electrodes (grid and anode), C_{ga}, partly of the capacitance contributed by the sharp edges of these electrodes, and by the capacitance of the two end surfaces. The two latter together constitute C_s. The capacitances C_{ga} and C_s depend in a complex way on the dimensions indicated in the figure. These dimensions are so chosen as to achieve the desired value of the product $P \times B$. This choice is also influenced, however, by the following considerations:

1) The resonant cavity must be tunable to the required frequency.
2) The distance d_{ga} must not be unduly large; otherwise the anode voltage required might become too high, which may result in a drop in efficiency.
3) The distance h between the anode bush and the grid disc (see fig. 1) cannot, for constructional reasons, be reduced *ad libitum*.
4) The product $G \times B$ must have a reasonable value.

Another important factor which limits the possibilities at high frequency is the permissible dissipation of grid and anode. The higher the frequency f at which the cavity is to resonate, the smaller must be the dimensions, the latter being inversely proportional to the frequency for geometrically similar resonant cavities. The surface area of the anode must therefore be inversely proportional to f^2. If we compare tubes of the same power output at different frequencies, we can speak of "equivalence" if the *relative* bandwidth is the same; the required value of the product $P \times B$ for such "equivalent" tubes is thus proportional to the frequency. Since the cavity dimensions vary inversely with the frequency, the factor $d_{ga}a^2C_{ga}/(C_{ga}+C_s)$ in equation (4) clearly varies according to f^{-3}; hence J^2 must vary according to f^4, i.e. the required J is proportional to f^2. Since the anode (and the cathode) area is proportional to f^{-2}, the total current, and consequently (see (2)) the voltage, too, remain independent of the frequency.

We see, then, that the specific anode dissipation increases with the square of the frequency in the case of "equivalent" tubes. If the materials for anode and grid are suitably chosen, however, the power to be dissipated is not a serious limiting factor in the design of tubes for the range around 4000 Mc/s. The specific anode dissipation in the EC 59 is 780 W/cm², the total dissipation being 125 W. The heat generated is dissipated by a water-cooling system.

Another point of consideration is the glass of the tube envelope which, being in the high-frequency field of the resonant cavity, might be heated to the softening point as a result of dielectric losses. This must obviously be avoided. The calculation for the resonant cavity with $h = 4$ mm shows that a generated power of $P = 1500/f$ (P in watts, f in 10^9 c/s) is permissible in the case of glasses for which $\varepsilon_r \tan \delta \approx 3 \times 10^{-3}$. At 4000 Mc/s this implies a maximum permissible high-frequency power of 400 W. It is clear, therefore, that the heating of the glass imposes no limitations on the design of the EC 59 triode.

Design of the EC 59 tube

The first step in dimensioning the tube was to determine the current density required from the cathode. With the L cathode it was found possible to set the current density J at 1.5 A/cm² (this operating current must of course be lower than the saturation current); at this value the tube can operate at a normal cathode temperature, which is important if it is to have a reasonable life. With a cathode-grid distance $d_{kg} = 0.06$ mm, we then have according to (1): $\tau_{kg} = 1.07 \times 10^{-10}$ sec, which at 4000 Mc/s corresponds approximately to $\tau_{kg}/T = 0.4$. Taking a cathode of diameter $2a = 4.5$ mm, and aiming at a value for $P \times B$ of 2×10^9 watt c/s, we find with the aid of (4):

$$a\, d_{ga} \frac{C_{ga}}{C_{ga}+C_s} = 1.75 \times 10^4 \text{ cm}^2/\mu\text{F}.$$

The value of $C_{ga}/(C_{ga}+C_s)$ was taken as 0.3, which is larger than in the case of the triode EC 57, owing to the larger value of a. The value of $C_{ga}/(C_{ga}+C_s)$ fixes the grid-anode distance, d_{ga}, at 0.3 mm. The other dimensions of the resonant cavity (fig. 1) are then determined: $h = 5.5$ mm and $b = 13$ mm. With these dimensions the resonant frequency is higher than required; by adjusting a piston so as to vary the size of the cavity, the system can be tuned to the correct frequency.

At a grid-cathode distance of 0.06 mm and an anode current density of 1.5 A/cm², the mean potential in the grid plane will be about 7 V, according to equation (2). If we then select the anode voltage (500 V) and the grid bias (—5 V), we arrive at a value of the amplification factor. Since d_{ga} is already fixed, we are left with two variables for achieving this amplification factor; these are the diameter and the pitch of the grid wires. In this connection it must be taken into account that, if the pitch is made much greater than the distance between grid and cathode, the result will be non-uniform emission

("Inselbildung") of the cathode [5]. With regard to grid dissipation, which occurs when a large control signal is applied, it was found desirable to use a grid wire of not too fine a gauge. Having decided on 30 μ wire, it was necessary to choose a pitch of 130 μ in order to obtain the required amplification factor [6].

Fig. 2 shows a cross-section of the tube thus designed. The table below gives the principal dimensions and electrical data of the EC 59 compared with those of the EC 57.

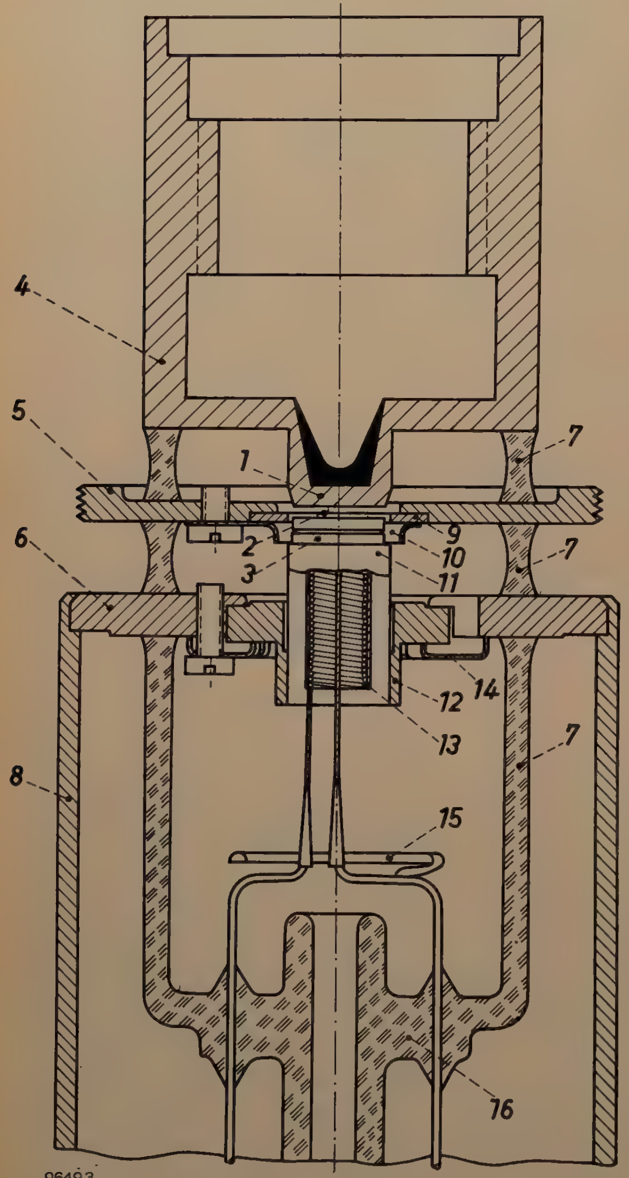

Fig. 2. Cross-section of disc-seal triode EC 59. *1* anode, *2* grid, *3* L cathode, *4* anode bush, *5* grid disc, *6* cathode disc, *7* three glass rings, *8* cathode bush, *9* grid frame, *10* shield, *11* Ta-foil cylinder, *12* cathode holder, *13* filament, *14* spring washer, *15* getter, *16* sintered-glass base.

	EC 57	EC 59
Cathode diameter $2a$	3 mm	4.5 mm
Grid-wire diameter	7.5 μ	30 μ
Pitch of grid wires .	48 μ	130 μ
d_{kg}	40 μ	60 μ
d_{ga}	240 μ	300 μ
J	0.84 A/cm²	1.5 A/cm²
$P\times B$	150 watt Mc/s	1000 watt Mc/s
$G\times B$	1600 Mc/s	1000 Mc/s

We see that with the EC 59 the product $P\times B$ is about 7 times larger than with the EC 57. The product $G\times B$ has dropped to about 60%, but at the required bandwidth of 100 Mc/s the tube still provides a gain of 10× (10 dB).

The above design considerations were based on a formula for the product $P\times B$ derived from the familiar theory applicable to low frequencies [7]. Furthermore, in determining the cathode-grid distance, use is made of the results of transit-time theory for small signals. The transit times in the case of *large* control signals give rise to the following additional effects.

a) In the space between grid and cathode the phenomenon of "back heating" occurs, causing a loss of emission. Owing to their finite transit time, the electrons emitted with a certain

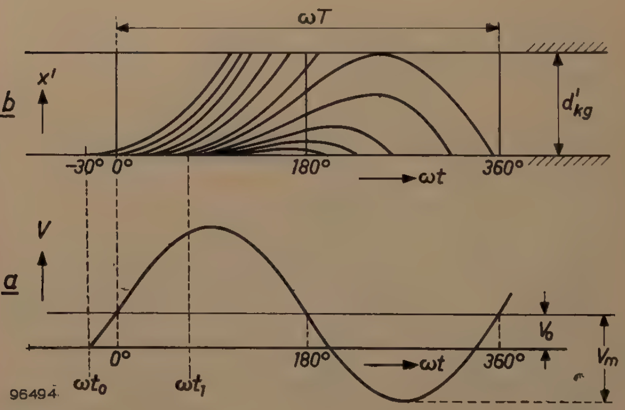

Fig. 3. *a*) Voltage V between grid and cathode (amplitude V_m, grid bias V_0) as a function of phase angle ωt.
b) Position x' between cathode and grid of electrons which have left the cathode at different instants within the duration $T = 2\pi/\omega$ of one cycle, plotted as a function of ωt. The transit time τ_{kg} from cathode to grid is *not* small with respect to T. In each cycle the phase ωt_0 of the first electron is determined by $V = V_0 + V_m \sin \omega t_0 = 0$, whence

$$\omega t_0 = -\sin^{-1}(V_0/V_m).$$

We have here class AB operation (see e.g. F. E. Terman, Electronic and radio engineering, McGraw-Hill, New York 1955, p. 255). The coordinate x' is a *reduced* coordinate, so that the figure is valid for arbitrary values of d_{kg}, V_0 and ω.

---

[5] This is due to a non-uniform potential distribution at the grid; immediately opposite the grid wires the field at the cathode may even change sign. The result is a reduction of the active emitting surface of the cathode.

[6] P. H. J. A. Kleijnen, Philips Res. Repts. 1, 81, 1946.

[7] See e.g. J. P. Heyboer, Transmitting valves, Philips Technical Library, 1951.

phase delay ωt_1 after the beginning of each cycle are no longer able to reach the grid, the effective potential in the grid plane having changed sign while the electrons are on their way (see *fig. 3*). These electrons therefore contribute nothing to the release of energy in the space between grid and anode, although they do absorb energy from the control signal, and they return to the cathode with a velocity which, in general, is greater than zero. With high negative grid bias, the phenomenon can assume inadmissible proportions. The best setting is found to be in the region of class B, which constitutes a favourable compromise between amplification and efficiency. (Back heating should not be confused with the phenomenon of total-emission damping, mentioned above.)

b) In a certain part of each cycle the electrons pass through the grid, and the first electrons do so at a greater speed than the later ones. Because of this their arrival on the anode is spread out over a greater part of the cycle than at the grid, resulting in a drop in efficiency.

c) The amplification decreases rapidly with increasing input power. This is due not only to the two phenomena mentioned above, which occur at high frequencies, but also to the fact that, (as at low frequencies), the grid intercepts part of the electrons during its positive period. These electrons, too, therefore contribute nothing to the transfer of energy to the grid-anode space. The grid current to which they give rise does not, however, call for more input power. In the grounded-grid circuit the input power is not affected by the presence of grid current, since the cathode-grid circuit is distinct from the grid-anode circuit [8]).

The mathematical treatment of these effects involves considerable difficulties, and it is therefore not possible to allow for them systematically in a design.

Engineering problems

The shape of the tube (*fig. 4*) is largely determined by the requirements imposed on the anode circuit. As we have seen, the anode-grid space is part of the output cavity of the amplifier in which the tube is incorporated. The electrode system is a planar structure with rotational symmetry. The anode proper is visible in the photograph as a small protrusion below the anode bush. In the amplifier the resonant cavity is further bounded by the cylindrical side walls of the block into which the tube is screwed, by the grid disc, and at the top by a piston; between the piston and the anode bush is an annular gap which forms a $\lambda/4$ transformer, coupling the cavity to the output waveguide. The diameter of the anode bush and of the glass spacer ring between it and the grid disc must be smaller than the dimension $2b$ of the resonant cavity (fig. 1). The diameter of the cathode bush is larger than that of the grid disc, but it should still be small enough to prevent resonance modes of higher order occurring in the high-frequency cathode "choke" [9]). These considerations determine the diameters of the bushes (see figs. 2 and 4).

The anode circuit losses must be kept as low as possible. All surfaces should be well polished and be good conductors. The screwed connections between the tube and the different parts of the amplifier should also be mechanically and electrically sound. The anode bush is hollow and open at the top (*fig. 5a*), so that it can be water-cooled. The inside of the bush is threaded, allowing screw attachment of the inner conductor of a coaxial system; the water-cooling channels run through this inner conductor (see fig. 5*b*). The anode construction adopted allows a certain freedom in the design of this cooling system.

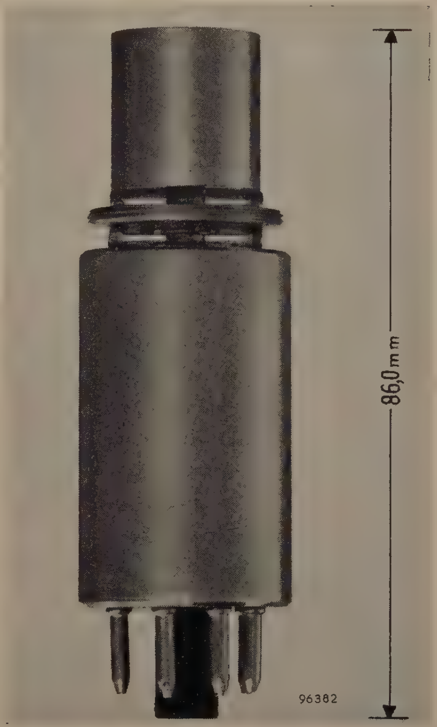

Fig. 4. The disc-seal triode EC 59. From top to bottom: anode bush, grid disc with screw-thread, cathode bush and pins in glass base. Through the glass spacer rings the actual electrodes can be seen.

Construction and assembly of the tube

To meet the requirement of good heat conductance, the anode is made of molybdenum provided with gold plating. The grid and cathode discs are made of an alloy of iron, nickel and cobalt ("Vacon 12") and are also gold-plated. The glass used between the electrodes has particularly low dielectric losses. These glass rings, and a glass cylinder underneath the cathode disc, are sealed in a jig

---

[8]) See e.g. W. Kleen, Einführung in die Mikrowellen-Elektronik, I. Grundlagen; Hirzel, Stuttgart 1952.

[9]) See e.g. J. P. M. Gieles, A 4000 Mc/s wide-band amplifier using a disc-seal triode, Philips tech. Rev. **19**, 145-156, 1957/58 (No. 5), especially p. 146.

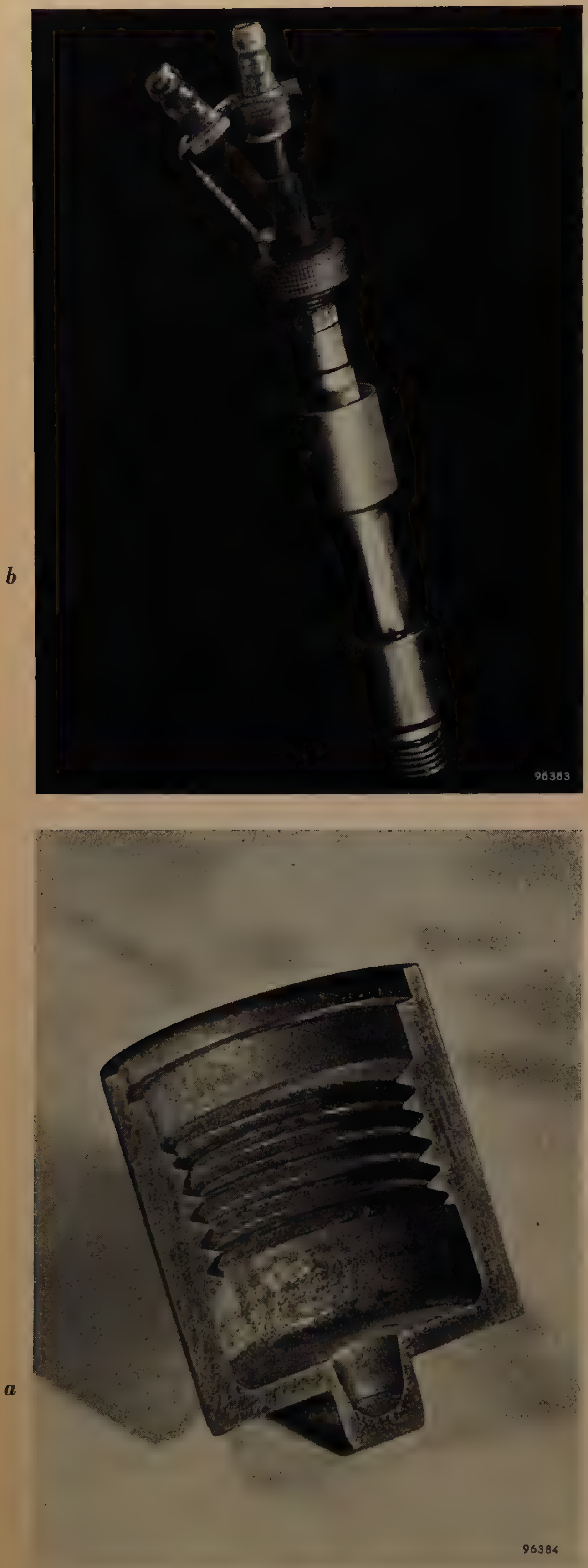

Fig. 5. *a*) Cut-away anode bush of the EC 59; *b*) inner conductor of coaxial system which is screwed into the anode bush, and through which the cooling channels pass (this is thus a component of the amplifier).

to the previously enamelled discs. The resultant assembly (*fig. 6a*) is set up on a precision lathe. The anode surface is machined flat, and the seatings are cut for the grid and the cathode holder. The distance between these faces must be very accurately adjusted. This is done by means of dial gauges (see *fig. 7*) mounted on the lathe. On the outside of the tube the thread is cut into the grid disc and the cathode disc is machined to size. All these operations are performed without moving the position of the assembly on the lathe, so that all surfaces are parallel and concentric. The grid is constructed by the method described in an earlier article [1]).

As mentioned, the cathode is of the L type. A molybdenum cylinder with a diametral wall forms two chambers. In the upper (smaller) chamber a tablet of barium-strontium carbonate is inserted, and a flat porous plate of tungsten is welded over the end. The filament is introduced into the lower chamber. A cylinder of tantalum foil (10 μ wall thickness) is fixed around the molybdenum tube and welded to the gold-plated "Vacon" holder. Fig. 6*b* shows the individual components and, on the left, the completely assembled cathode. Note the machined face on the cathode holder which is pressed against the cathode disc, and which determines the grid-cathode distance. To make this face parallel with the cathode surface, the cathode assembly is set up on a lathe via a universal joint. With a highly sensitive dial gauge, adjustments are made until the cathode surface is perpendicular to the axis of rotation. The thrust face of the cathode holder is then machined to produce the exact required distance between the face and the cathode surface. The accurate parallel alignment thus obtained is demonstrated by the fact that only very slight differences are found between the static characteristics of one tube and another.

Like the EC 57, the EC 59 is assembled under a dust cover. After the envelope has been de-burred and cleaned, and the spacings again checked, the grid is fixed to the grid disc by means of screws. The cathode holder is then mounted and pressed against the seating in the cathode disc by a spring-loaded washer. A sintered-glass base with filament and getter (fig. 6*c*) is introduced into the glass cylinder and sealed to the glass, after which the tube is pumped and sealed off. A photograph of the finished tube can be seen in fig. 6*d*. The cathode cylinder is now rimmed onto the cathode disc on a lathe; in this way any possible excentricity is kept within fine limits.

Finally the tube is aged and subjected to static and dynamic tests.

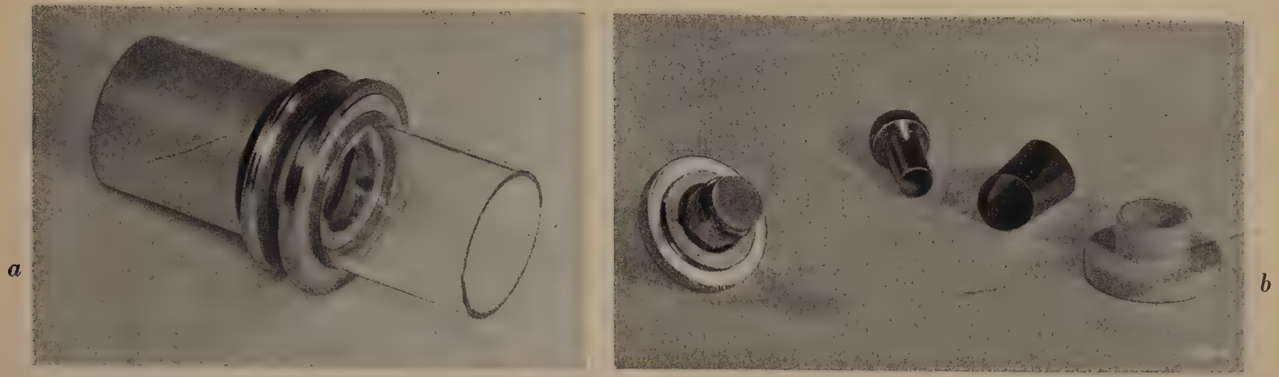

Fig. 6. Components of the EC 59 in various stages of fabrication.
a) Anode bush, grid disc and cathode disc sealed to glass.
b) From left to right: assembled cathode, molybdenum cylinder, tantalum-foil cylinder and unmachined cathode holder.
c) Filament and getter ring on sintered-glass base.
d) Grid and cathode mounted, sintered-glass base with filament sealed in, and tube evacuated.

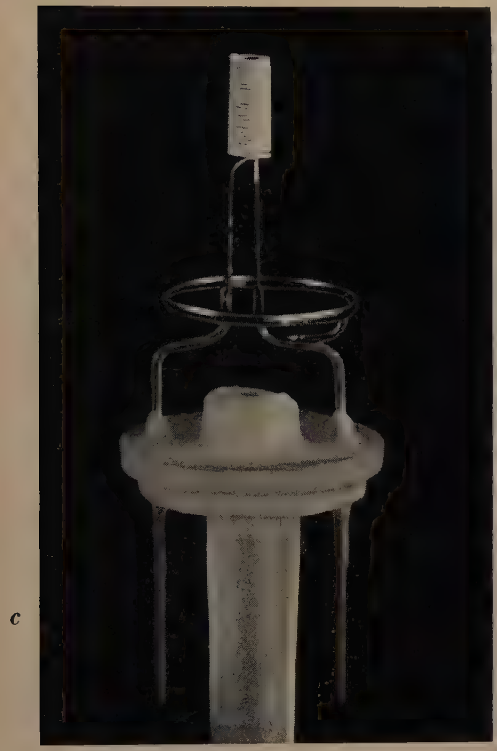

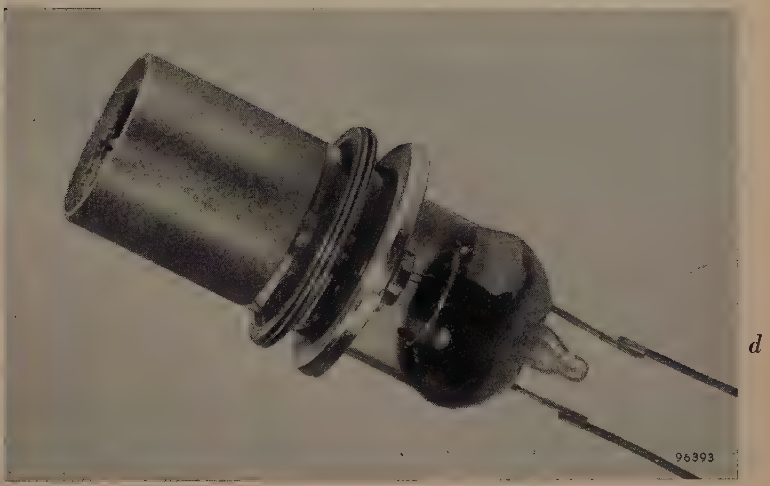

Fig. 8 shows two tubes under static loading, cooling being provided by a closed water-circuit. The water reservoir with radiator and pumping motor are in the foreground. The water in the reservoir is kept at a temperature of about 50 °C. The advantage of this system is that the water is never below room temperature when it enters the cooling system, so that there is no risk of arcing being caused by condensation on the anode bush. Moreover, water at higher temperature has a better coefficient of heat transfer.

The set-up for life testing under dynamic load is shown in *figs. 9* and *10*. The signal from the oscillator (left) passes via an attenuator to the amplifier on the right. The tube is not visible, being completely enclosed in the amplifier block. The output signal is passed via an attenuator to the next amplifier stage. There are thus several amplifiers connected in series, so that with a single oscillator it is possible to test a series of transmitting tubes at the same time. The attenuators are adjusted so that each amplifier can deliver an output of 10 W for an input power of about 1 W.

Another version of this tube is at present being developed in Hamburg, employing *ceramic* instead of glass seals; this tube will be described in a forthcoming article. Furthermore, by slightly modifying the anode design, it has proved possible to cool the EC 59 with *air* instead of water. At an anode dissipation of 115 watts the air-cooling system maintains

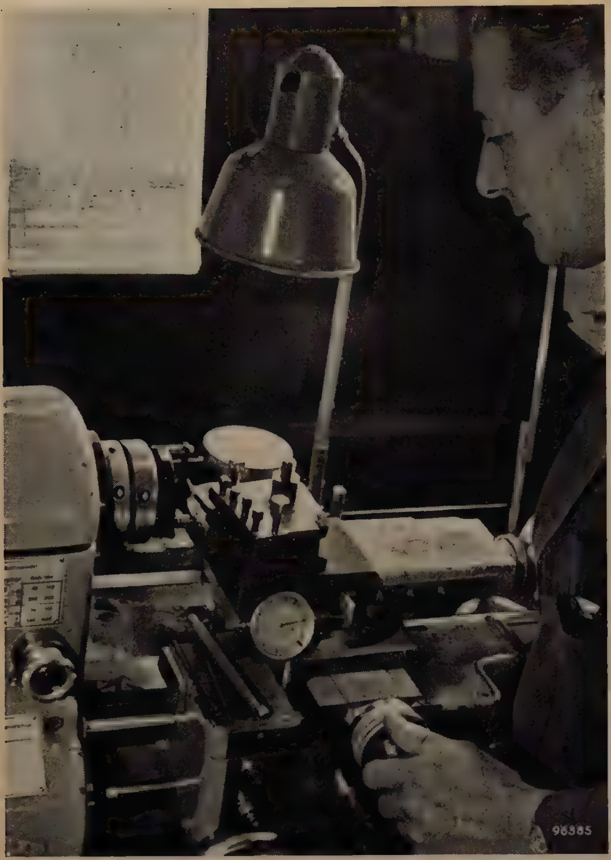

Fig. 7.

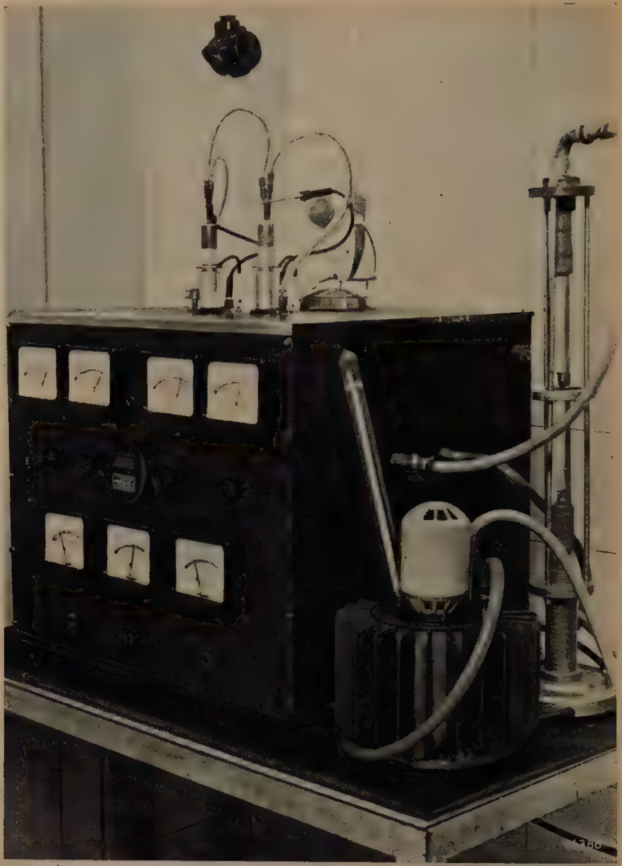

Fig. 8.

Fig. 7. Machining the thrust face in the cathode holder.
Fig. 8. Experimental arrangement for static life-tests, the tubes being cooled by a closed water circuit. Two EC 59 tubes are on the top of the cabinet. Bottom right are the water reservoir with cooling fins, circulation pump and thermometer.

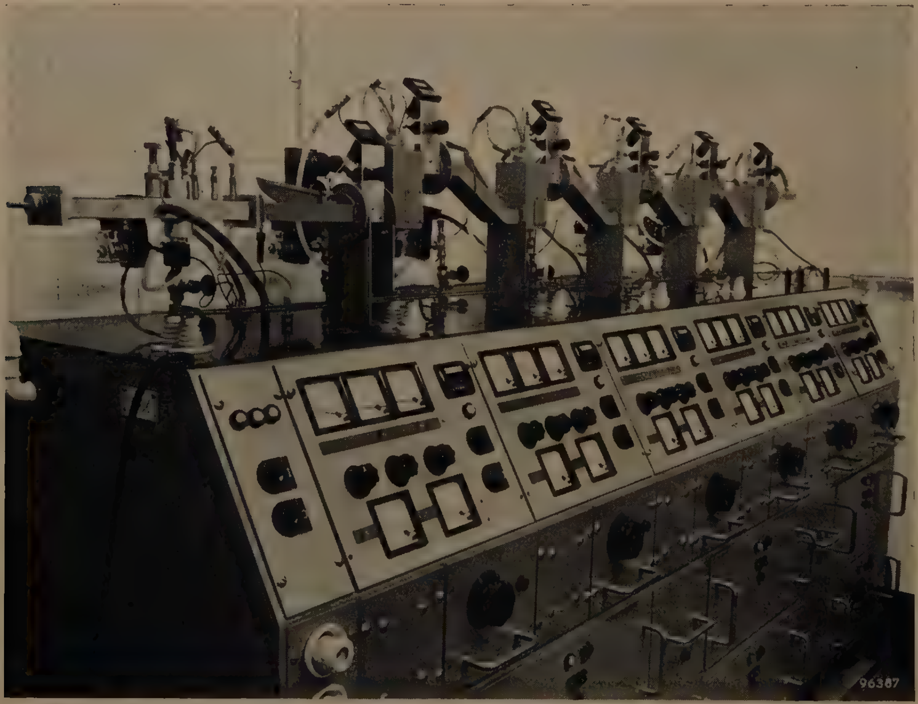

Fig. 9. Arrangement for dynamic life-tests. The tubes operate day and night under the same conditions as in normal use.

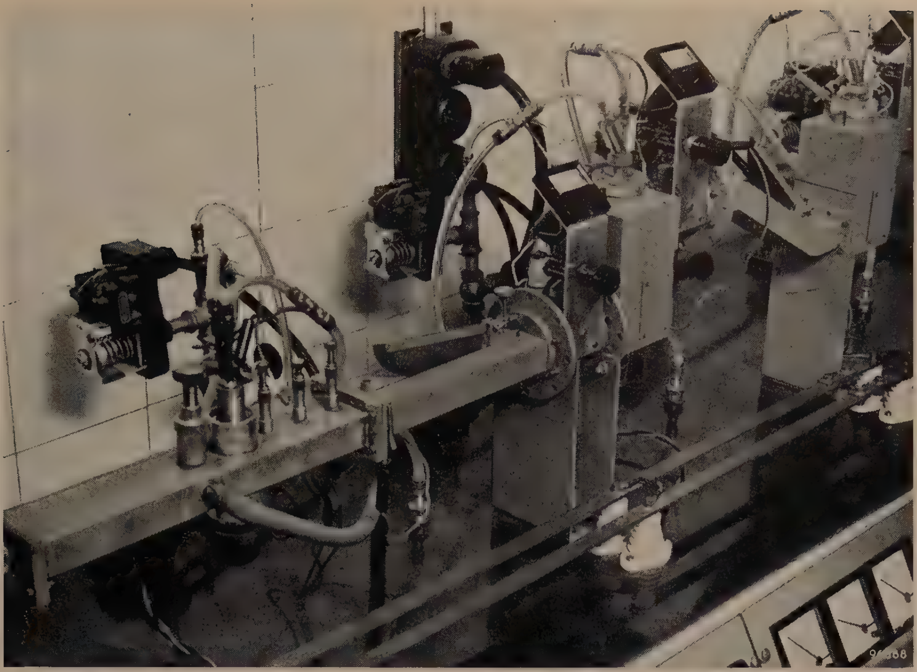

Fig. 10. Detail view of the set-up for dynamic life tests. Left, the oscillator; right, the first two amplifying stages containing type EC 59 tubes.

the temperature of the anode at 120 °C above room temperature at the position of the glass seal. The quantity of air required is then 75 l/min at a pressure of 47 cm water. The cooling method preferred will depend on local conditions.

Summary. In the design of a microwave transmitting triode the fundamental requirement is a relatively short electron transit time in the cathode-grid space. For the tube to operate at very high frequencies, the distance between grid and cathode must therefore be extremely small (some tens of microns) and the cathode current density very high. In these respects the L cathode constitutes an important step forward. At a given current density, the product of bandwidth and output power is mainly determined by the geometry of the tube. A large power-bandwidth product depends, among other things, on minimizing the capacitance between grid and anode. Another important factor is the specific anode dissipation, which rises with increasing frequency. The disc-seal triode EC 59, which is a further development of the earlier described type EC 57, can deliver a high-frequency power of 10 W at 4000 Mc/s over a bandwidth of 100 Mc/s and at a power gain of about 10 dB. The tube is water-cooled (air cooling is also possible). The extremely small clearances between the electrodes are adjusted during fabrication by first sealing the anode bush and the grid and cathode discs in the glass spacer rings and then machining on a precision lathe the seatings into which the actual electrodes are subsequently fitted. In this way the disposition of the electrodes is very accurately fixed. A description is given of the design and fabrication of the tube, and brief mention is made of the cooling system and the method of life testing.

PRECISION VARIABLE CAPACITORS

by A. A. TURNBULL *).

621.319.43

Electronic equipment for military uses is designed for specifications which require components of very high quality. Components must frequently be not only of high accuracy and stability but must also be compact and robust. The article below describes two precision variable capacitors which, although compact, have a performance comparable with laboratory capacitors of considerably larger size.

Two types of precision variable capacitors (*fig. 1*) have been designed at the Mullard Research Laboratories for high grade electronic equipment, meeting stringent specifications as regards their accuracy and stability [1]. One of these capacitors gives a linear frequency law for use in transmitter master-oscillator circuits or in receiver local oscillator circuits. The other is a sine-frequency-law capacitor and was designed primarily for the conversion of radar range and bearing information from polar to cartesian form [2].

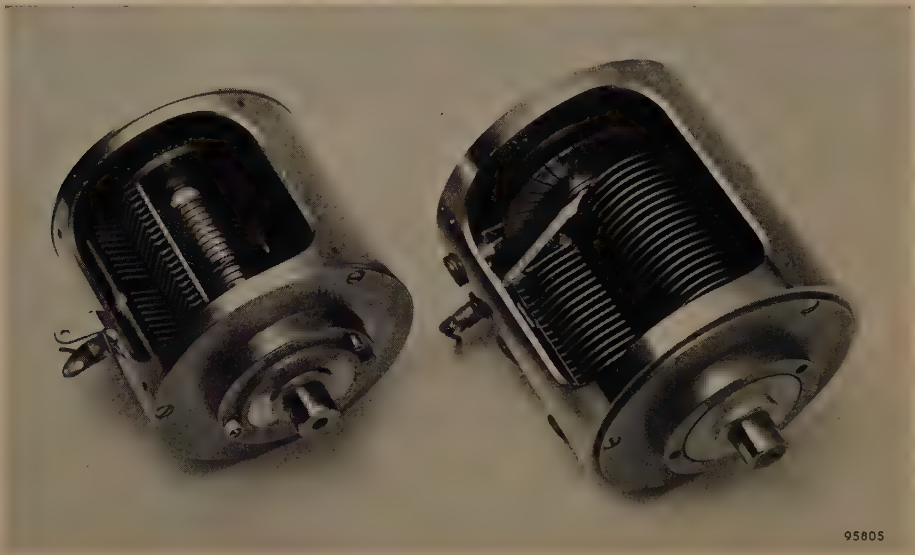

Fig. 1. The two precision capacitors with covers removed. Left, the linear-law capacitor. Right, the sine-law capacitor.

The term stability in connection with these capacitors implies stability over long periods, stability with respect to temperature variations and with respect to vibration. In addition close limits are imposed on any deviation from the relevant frequency law, and the capacitors must also possess a high degree of re-settability. A further requirement is that the capacitors should be sufficiently small to allow their convenient installation in equipment, particularly in compact military equipment. The linear-law capacitor, for example, was originally designed for a specific equipment, in which three of these capacitors were ganged in line. In the layout of this equipment only a limited space was available for the capacitors. Similar considerations also limit the size of the sine-law capacitor.

Some of the features common to both the capacitors may be described, before passing on to the detailed consideration of each type. As stability was the primary consideration in design, structural rigidity is essential. For this reason the capacitors are mounted in a robust cylindrical case with an aperture to permit access to the vanes during assembly. A cover to fit over this aperture is provided for electrical screening and dust protection. A substantially mono-metallic construction is used which avoids stresses being set up due to differential expansions. In certain versions of the linear capacitor one of the rotor vanes is replaced by a bimetallic vane to increase stability in cases where the equipment is not temperature-regulated. This will be discussed further below.

---

*) Mullard Research Laboratories, Salfords, Surrey, England.

[1] A brief description has been published in Brit. Comm. and Electronics 4, 756-759, 1957.

[2] British Patent No. 764 478.

Mechanical play in the rotors of the two capacitors has been practically eliminated by the use of high-precision angular contact ball-bearings (see below) in which the eccentricity is less than 0.0001 inch. The rotor is mounted in such a way that there is a certain axial and radial load on the bearings; in this way both axial and radial slackness are taken up and no play is possible.

Instability of electrical origin, such as varying surface conductivity or varying dielectric losses in the insulators, is minimized by the use of high-grade ceramic insulators. These support the stator vanes, the rotor vanes being mounted on the earthed rotor assembly.

The temperature coefficient of capacitance is determined largely by the linear temperature coefficient of expansion of the metal used. For both capacitors brass is used for most of the metal parts: this results in a temperature coefficient of capacitance of +18 ±5 parts per million per °C.

The shape of the vanes differs, of course, in the two capacitors. The shapes required for the linear law and for the sine law were first calculated theoretically. Considerable experimental work was necessary, however, to obtain the correct vane shapes to ensure precise conformity to the ideal curves.

Furthermore, in order that these accurate frequency laws are maintained from one capacitor to another in production, particular care is necessary in the choice of materials for the vanes and in the application of precision techniques for assembly. Stator and rotor vanes are assembled in special jigs, as will be described presently.

Design of the linear law capacitor

The linear-law capacitor is designed for use in oscillator circuits in which a frequency coverage of two to one is required for a capacitance change of about 300 pF. This is obtained in the present design with an angular rotation of 150°. Over this range the capacity conforms to the ideal linear law within ±0.05% in frequency. Furthermore the *rate* of deviation from the ideal law is nowhere greater than 0.02% in frequency per 5° shaft rotation.

The general layout of the linear-law capacitor can be seen from the schematic diagram of *fig. 2*. The stator vane packet is supported on three supports, two being ceramic pillars and the third a glass-metal seal assembly which forms part of the stator terminal. The electrical connection to the rotor assembly is made by a wiper mounted in the centre of the rotor shaft. The use of a central wiper minimizes the self-inductance of the capacitor. The wiper consists of two rhodium-flashed beryllium-copper wires spring-loaded into a locating groove in the shaft. The rhodium plating gives low contact resistance and good wearing properties. The wiper is connected to the central wire of a coaxial connector using "Fluon" (polytetrafluorethylene) insulation. Normally the capacitor is used with the wiper connected to the case, except when special versions are used in which the shaft is insulated from the case with ceramic spacers.

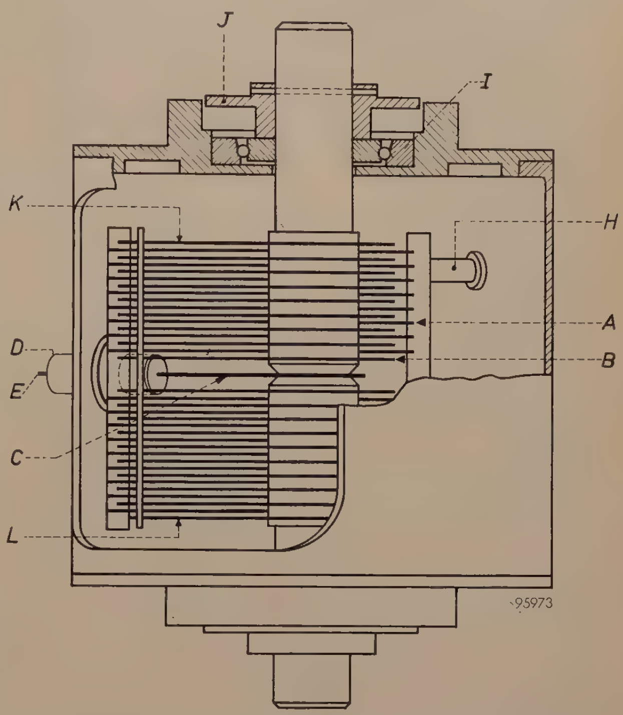

Fig. 2. Simplified cross-section of the linear-law capacitor. *A* stator vanes, *B* rotor vanes, *C* rhodium-plated beryllium-copper wiper wire, *D* stator terminal, *E* rotor terminal, *H* ceramic insulator, *I* angular-contact ball-bearing, *J* bearing thrust collar with locking pin through shaft, *K* trimmer vane, *L* second trimmer vane (uncompensated versions) or bi-metal vane (temperature-compensated versions).

Temperature compensation

For certain applications, for example where it is not practicable to mount the capacitor in temperature-regulated surroundings, it is desirable to provide some measure of temperature compensation. In some models of the linear-law capacitor, therefore, the last vane at one end of the rotor is replaced by a bi-metal vane, which gives the capacitor a temperature coefficient of about —15 parts per million per °C near the maximum capacitance setting. The negative temperature coefficient obtained with this bi-metallic vane reduces short-term instability of oscillator circuits due to variation in temperature by approximately compensating the normally positive temperature coefficients associated with the coil in the circuit. (With care and using selected materials it is possible to construct coils having a positive temperature coefficient as low as +15 p.p.m./°C.)

The figure of —15 p.p.m./°C for the temperature coefficient of the capacitor refers to the maximum setting of the capacitor. The temperature coefficient near the minimum capacitance settings will not be effective in compensating temperature variations in the coil inductance since, here, the capacitance of the variable capacitor in circuit is a much smaller proportion of the total circuit capacitance. Approximate temperature compensation of the oscillator at the minimum capacitance setting can be effected by placing in parallel with the variable capacitor a fixed capacitor C_p whose temperature coefficient is so chosen that near the minimum setting of the variable capacitance the overall circuit-capacitance temperature coefficient is —15 p.p.m./°C. The overall circuit capacitance then comprises (*fig. 3a*) the minimum capacitance of the variable capacitor C_v, the fixed parallel capacitance C_p, and the stray circuit capacitance C_s. On now rotating the variable-capacitor shaft to near its maximum setting where its temperature coefficient of capacitance is nominally —15 p.p.m./°C, the overall circuit temperature coefficient of capacitance deviates only slightly from —15 p.p.m./°C.

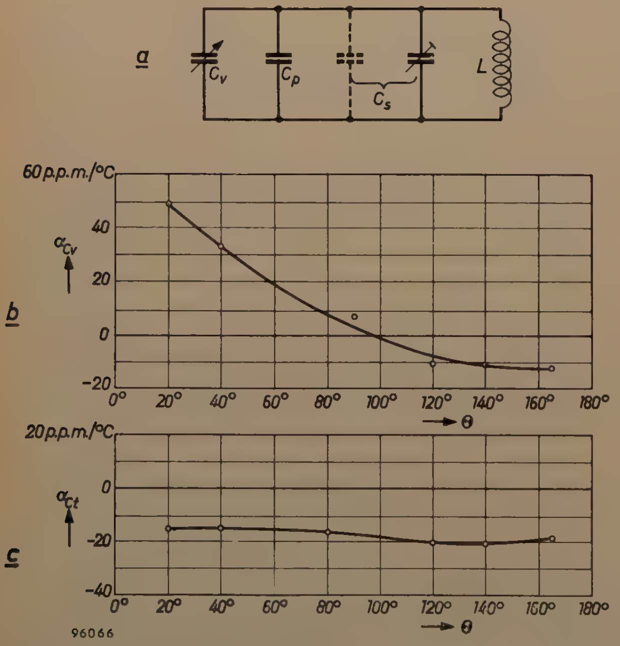

Fig. 3. Temperature compensation of linear-law capacitor.
a) Tuned circuit consisting of the variable capacitor C_v, a fixed parallel capacitor C_p, the stray circuit-capacitance plus that of a trimmer C_s and a coil L.
b) Variation of the temperature coefficient α_{C_v} of the variable capacitor with angular setting of the shaft.
c) Variation of total circuit capacitance α_{C_t} with angular setting of shaft.

In fig. 3*a*, C_v is the capacitance of the variable capacitor, C_s is the stray circuit capacitance plus the capacitance of a trimmer, and C_p is the fixed parallel capacitance, of such a value that the total capacitance in parallel with C_v is $C_p + C_s = 65 \pm 1$ pF. (This value is the parallel capacitance necessary to correct the variable capacitor and thus give precise conformity with the linear frequency law. Adjustment to the precise value between the limits ±1 pF is effected by an empirical method.)

From $f = L^{-1/2} C^{-1/2}/2\pi$ it follows (T = temperature) that:

$$\frac{\mathrm{d}f}{\mathrm{d}T} = \frac{1}{2\pi}\left[-\tfrac{1}{2}L^{-3/2}C^{-1/2}\frac{\mathrm{d}L}{\mathrm{d}T} - \tfrac{1}{2}L^{-1/2}C^{-3/2}\frac{\mathrm{d}C}{\mathrm{d}T}\right] =$$

$$= -\tfrac{1}{2}\left[\frac{f}{L}\frac{\mathrm{d}L}{\mathrm{d}T} + \frac{f}{C}\frac{\mathrm{d}C}{\mathrm{d}T}\right].$$

If now we let α_f denote the temperature coefficient of frequency f, α_{C_t} the temperature coefficient of the total circuit capacitance C_t and α_L the temperature coefficient of the coil inductance, then

$$\alpha_f \equiv \frac{1}{f}\frac{\mathrm{d}f}{\mathrm{d}T} = -\tfrac{1}{2}(\alpha_L + \alpha_{C_t}).$$

Since α_L is approximately +15 p.p.m./°C, we require that α_{C_t} be approximately —15 p,p,m./°C in order that α_f may be approximately zero. The manner in which the temperature coefficient α_{C_v} of the variable capacitor itself varies with the angular setting of the rotor is shown in fig. 3*b*. If now the temperature coefficient α_{C_p} of the fixed parallel capacitance is adjusted (see below) such that at, say, the angular setting 20°, the temperature coefficient α_{C_t} of the total circuit capacitance is nominally —15 p.p.m./°C, then α_{C_t} will vary with the angular setting of the rotor as shown in fig. 3*c*.

It can be seen that the maximum value of α_{C_t} is approximately —21 p.p.m./°C. At this point therefore, for α_L equal to +15 p.p.m./°C, α_f would be $-\tfrac{1}{2}(+15-21) = 3$ p.p.m./°C. This simplified outline of the method of temperature compensation, which ignores such factors as possible variations of α_L with frequency, shows that it is possible with sufficient care to effect temperature compensation to within 3 p.p.m./°C over the whole frequency range.

It should be added that figs. 3*b* and *c* refer to a single typical capacitor employing a bi-metallic compensating vane. However (see *Table I* below), there is a spread of ±10 p.p.m./°C in the temperature coefficient as between actual manufactured capacitors, near the maximum capacitance setting. Taking this factor into account it may not always be possible to effect the temperature compensation of an oscillator to within 3 p.p.m./°C but it should always be possible to achieve compensation to within 10 p.p.m./°C (in frequency).

When the required temperature coefficient of C_p has been calculated, one method whereby it may be adjusted to the required value is to make C_p comprise two fixed capacitors in parallel. One of these capacitors would normally be a high-grade silvered-mica capacitor and the other a relativily small-valued capacitor of silvered-ceramic construction. Since silvered-ceramic capacitors with a fairly wide

Table I. Summarized specification for linear-law precision variable capacitor.

Capacitance at 0°	20.0 ± 1 pF
Capacitance variation for 2 : 1 frequency range (for angular swing 26°-176°)	292.8 pF
Conformity to linear law (with optimum parallel capacitance) .	± 0.05 % in *frequency*
Self-inductance	0.015 μH
Power factor at maximum capacitance, measured at 1 Mc/s . .	< 0.00005
Insulation resistance (stator to rotor)	> 1000 MΩ
Breakdown voltage measured at 50 c/s	> 500 V r.m.s.
Torque	< 6 oz.in. [<450 g.cm = 0.044 N.m]
Temperature coefficient near maximum capacitance:	
for uncompensated versions . .	+ 18 ± 5 p.p.m./°C
for compensated versions . . .	− 15 ± 10 p.p.m./°C
Dimensions:	
overall length	4.4 in.
overall width	3.0 in.

range of known positive or negative temperature coefficients are obtainable, it is usually possible by selecting a suitable capacitor of this type to achieve the correct temperature coefficient of the overall circuit capacitance at the minimum setting (20°) and hence temperature compensation of frequency over the whole range.

Design of the sine-law capacitor

The frequency law of the sine-law capacitor is such that when the capacitor is connected in a suitable oscillatory circuit the oscillator frequency varies sinusoidally about a mean value as the rotor shaft is rotated continuously. This variable frequency may be expressed as:

$$f_\Theta = f_{\mathrm{m}} + f_1 \cos \Theta,$$

where f_Θ is the oscillator frequency for the setting Θ of the shaft and f_{m} is a fixed frequency. To convert polar coordinates in a radar system to cartesians, which was the use for which this capacitor was originally designed, the capacitor shaft is arranged to rotate in synchronism with the radar aerial direction Θ while the capacitor forms part of the frequency-determining circuit of a variable-frequency oscillator. By beating the sinusoidally frequency-modulated signal $f_\Theta = f_{\mathrm{m}} + f_1 \cos \Theta$ with the signal from a fixed-frequency oscillator of frequency f_{m}, the resultant difference frequency is $f_1 \cos \Theta$.

If now a suitable gate is opened at the time the radar transmitted pulse sets out, and closed again at the moment the radar echo is received, the number of cycles performed by the oscillator (which can be directly counted) will be proportional to both the range R of the target and also to $\cos \Theta$ (*fig. 4*).

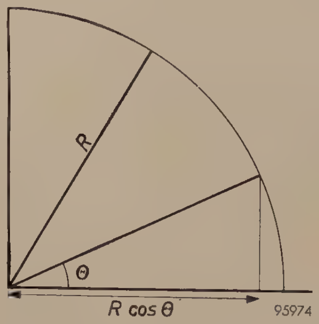

Fig. 4. Conversion of radar data from polar coordinates to cartesians, using the sine-law capacitor to produce a signal of frequency porportional to the cosine of the angular position of the radar aerial. The time interval between transmission of a pulse and reception of its echo is proportional to the range R. Hence for all points at a given range (R, say) this time is the same. Since, however, the frequency of the signal transmitted in any direction Θ is proportional to $\cos \Theta$, the number of cycles counted in the above-mentioned time interval is in each case proportional to $\cos \Theta$, so that this number of cycles is a measure of the x-coordinate $R \cos \Theta$. A similar arrangement generates the y-coordinate $R \sin \Theta$.

A second variable capacitor ganged 90° out of phase with the first and forming part of a second oscillatory circuit enables $R \sin \Theta$ to be generated.

The design of the sine-law capacitor follows the same general lines as the linear-law capacitor. The main differences are in the vane packets and in the wiper, which now has to stand up to continuous rotation. This capacitor is somewhat larger than the linear-law capacitor. The general layout is shown in *fig. 5*.

As with the linear capacitor, the shape of the vanes was derived theoretically and then the precise profile determined with the aid of experimental data. In this way it is possible to construct capacitors whose capacitance is accurate at all settings to within ±0.02% of the maximum capacitance.

To obtain the conformity to within these close limits, two extra vanes termed the corrector vane and the trimmer vane are added to the rotor and also two small stator vanes termed stator flags are present (their location is shown in fig. 5). *Fig. 6* shows the shape of the vanes. The corrector vane is used to give a coarse correction to the overall capacitance law to within ±0.96 pF for all angular settings. The final correction is made by adjusting the segments of the trimmer vane. This vane has a circular profile with 36 radial slots (see also fig. 1; the corrector vane is behind the trimmer vane in this photograph and is therefore not visible). It will be noted from fig. 6 that all rotor vanes includ-

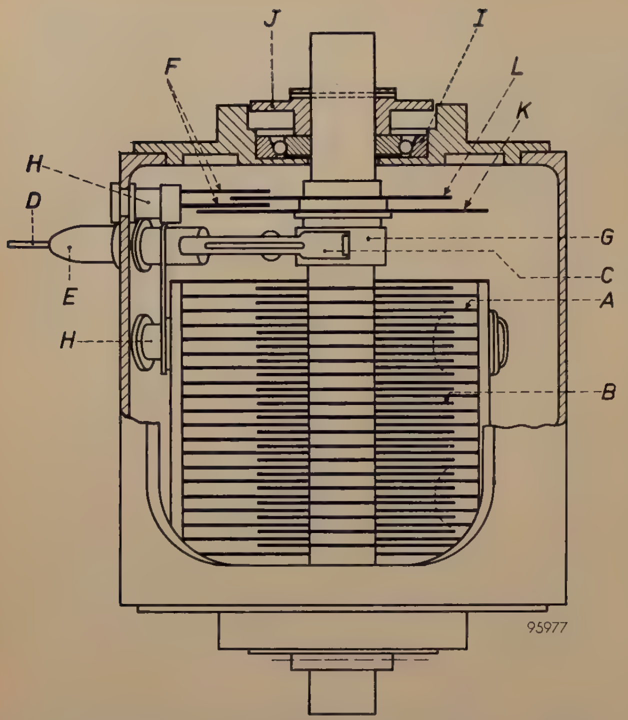

Fig. 5. Simplified drawing showing construction of sine-law capacitor. *A* stator vanes, *B* rotor vanes, *C* silver-graphite wiper brush, *D* stator terminal, *E* rotor terminal, connected to case, *F* stator flags, *G* silver slip ring, *H* ceramic insulators, *I* angular-contact ball-bearing, *J* bearing thrust collar with locking pin through shaft, *K* trimmer vane, *L* corrector vane.

ing the corrector and trimming vanes and the stator vanes are symmetrical about a central line, so that the law of the capacitor obtained as the rotor shaft is rotated from 0° to 360° is symmetrical about 180° (defining 0° to correspond to minimum capacitance).

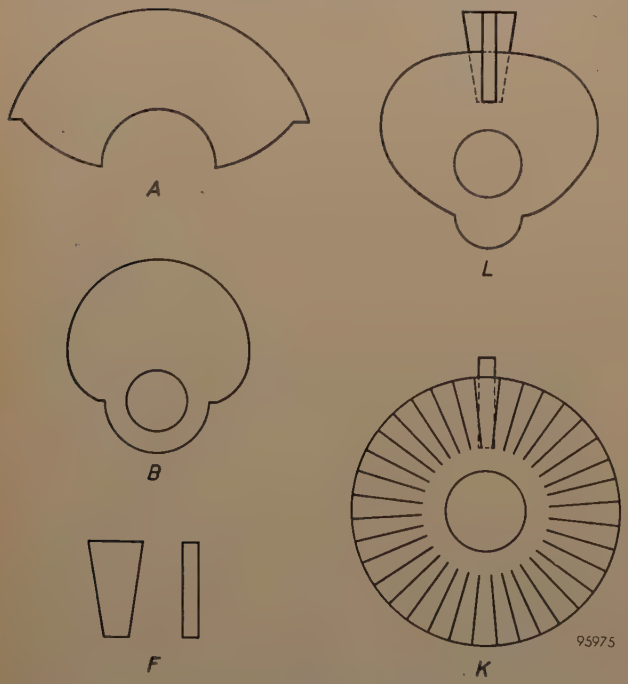

Fig. 6. Profiles of vanes in sine-law capacitor. *A* stator vane, *B* rotor vane, *E* the two stator flags, *L* corrector vane, showing relative positions of stator flags on either side of vane, *K* trimmer vane, showing relative position of the smaller stator flag.

The equipment for which this capacitor was designed provides temperature stabilization for the oscillator components. No bi-metallic temperature-compensating vane is therefore needed, although it is still necessary that the temperature coefficient of the capacitor should be small and held within close limits. In fact the temperature coefficient is held to within +18 ±5 p.p.m./°C at maximum capacitance (see *Table II*).

Table II. Summarized specification for sine-law precision variable capacitor.

Frequency law	$f_\Theta = f_m + f_1 \cos \Theta$, where f_m = 500 000 c/s and f_1 = 47 680 c/s
Capacitance at 0°	30.5 pF
Capacitance swing 0°-180° (and 180°-360°)	398 pF
Conformity to law	± 0.02 % of *maximum capacitance*
Power factor at maximum capacitance, measured at 1 Mc/s	< 0.0003
Torque	< 3 oz.in. [<225 g.cm = 0.022 N.m]
Temperature coefficient of capacitance	+18±5 p.p.m./°C
Dimensions:	
overall length	5.0 in.
overall width	3.25 in.

The sine capacitor has to be used under conditions of continuous rotation for exceptionally long periods without any significant wiper-bearing wear taking place. The design provides for a shaft rotation at a rate of 10 r.p.m. for not less than 5 million revolutions. To achieve this long life and to give a consistently low contact resistance (approximately 0.001 Ω), the capacitor uses a wiper consisting of silver-graphite brushes bearing on a silver slip ring (see fig. 5).

The stator vane packet is supported from the cylindrical case and insulated from it by four ceramic pillars. A further ceramic pillar supports the two stator flags. The capacitor terminals are coaxial, "Fluon" insulation being used for the stator connector.

Manufacture and assembly

The method of assembling the vanes consists basically of applying precision techniques to a fairly standard procedure. The principle involved is that of assembling the rotor shaft together with the rotor and stator vanes as one unit. The vanes are separated by spacer vanes and accurately jigged in their correct relative positions while the rotor vanes are soldered to the shaft and the tie bars to

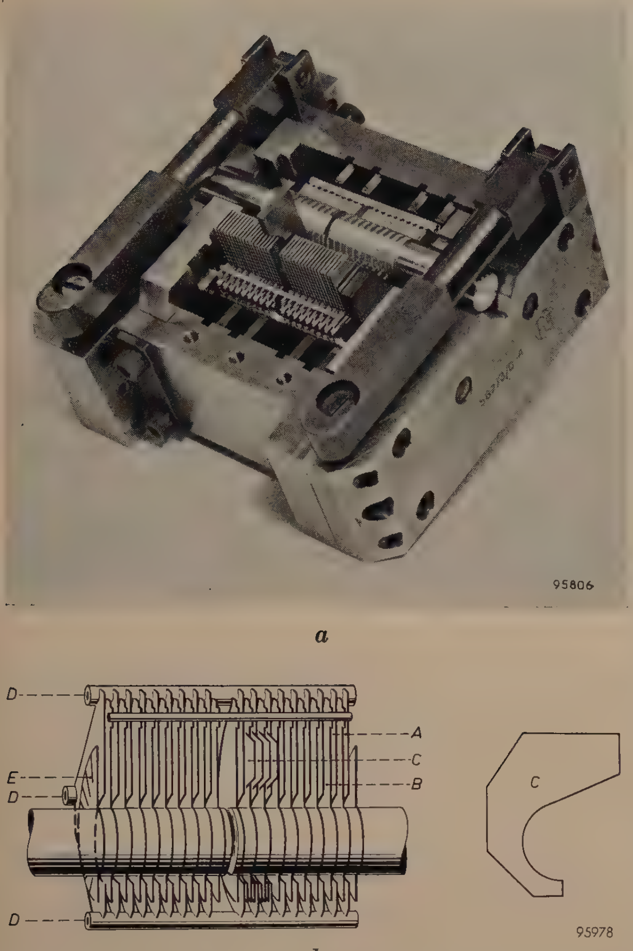

Fig. 7. *a*) Assembly jig with stator, rotor and spacer vanes in position. *b*) View of vane packet of linear capacitor after removal from jig. *A* stator vanes, *B* rotor vanes, *C* spacer vanes (only four shown in position, for clarity). *D* stator-vane tie bars, *E* trimmer vane. The shape of the spacer vanes is shown on the right.

the vanes. The jig used for this purpose is shown in *fig. 7a.* The sketch of fig. 7*b* shows a view of the assembly after removal from the jig. This assembly (with the spacer vanes still in position) is now mounted within the capacitor case. This is effected by locating the inner halves of the bearing races on the shaft and loading them on the outer races with a thrust of 40 pounds weight, which is applied to collars that are also located on the shaft and subsequently locked to the shaft with taper pins. At this stage the complete vane packet (i.e. including the stator vanes) is free to rotate with the shaft. The stator vane packet is then fixed to the insulated supports which are mounted on the capacitor case, by soldering the tie bars to the supports. In this manner, throughout the assembly of the capacitor, the accurate relative positioning of the rotor and stator vane packets is maintained. The final operation of removing the spacer vanes permits the shaft to be rotated.

The accuracy of the capacitors is determined to a very large extent by the tolerance on the thickness of the spacer vanes. The brass strip from which the spacer, rotor and stator vanes are blanked undergoes a process during its manufacture when the surface is shaved to yield a very close tolerance on thickness such that there are no greater variations than about 0.0004 inch from the nominal value and no greater variations in thickness over the whole area of any one metre long strip than 0.0001 inch. In order that the average rotor-to-stator spacing should be even more accurately controlled, one half of the spacer vanes used for any one capacitor are made of strip with a thickness error no greater than 0.0002 inch in *excess* of the nominal value while the other half are made from strip with the same error in thickness *less* than the nominal value.

For the linear-law capacitor the method of assembly of the rotor and stator vanes must be such that the resultant law of the capacitor, prior to adjustment by means of the trimmer vane, be within approximately 0.25% in frequency. Only then can the final adjustment by means of the trimmer vane be effected to the required tolerance of ±0.05% in frequency.

Both capacitors are mounted by clamping in a U-shaped cradle, a basic type of which is shown in *fig. 8a.*

A special flexible coupling has been designed for the purpose of ganging the capacitors to each other and to the drive shaft. A collar is attached to each shaft by means of grub screws, each collar being linked to a rigid outer rim by means of a flexible corrugated diaphragm (see fig. 8*b*). With the shafts aligned and set at the correct relative angle, the

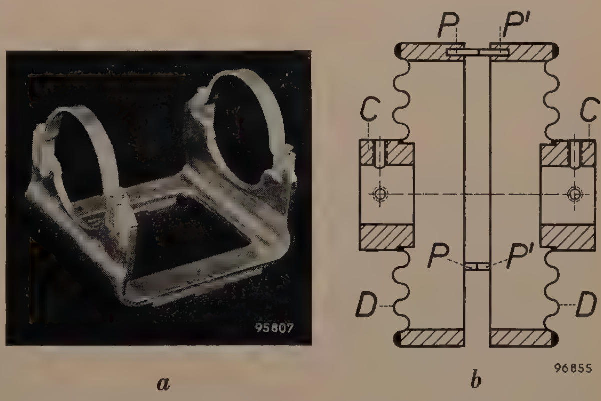

Fig. 8. *a*) Basic form of the mounting cradle for the precision capacitors. *b*) Flexible coupling used for ganging the shafts. The collars *C* of each half are locked with grub screws to the two shafts such that, with the shafts at their desired relative orientation, the three pins *P* are approximately aligned with the three pins *P.*′ After the grub screws have been tightened, the shafts are set *precisely* to the correct relative orientation and solder is run over the junctions of the pins. *D* are corrugated metal diaphragms.

two rigid rims are then locked together by running solder between the two sets of three pins. This procedure avoids the slight relative rotation between the two shafts that usually occurs when the grub screws of a coupling are tightened onto the shafts.

Performance and characteristics

The linear-law capacitor

Over a frequency range of 2 : 1 (a capacitance swing of approximately 300 pF), the linear capacitor conforms to the straight-line law to within ±0.05% in frequency as is required. *Fig. 9* is a graph for a typical capacitor showing how the errors vary with the angular setting of the shaft. It can be seen that nowhere do the errors exceed 0.05% in frequency between the angles 18° and 176°. The frequency coverage of 2 : 1 is obtained between the angles 26° and 176° (the same frequency coverage may also be obtained between other pairs of angles, such as 22° and 174° or 18° and 172°). As mentioned above, this performance is obtained when the total capacitance in parallel with the variable capacitors is 65 ± 1 pF.

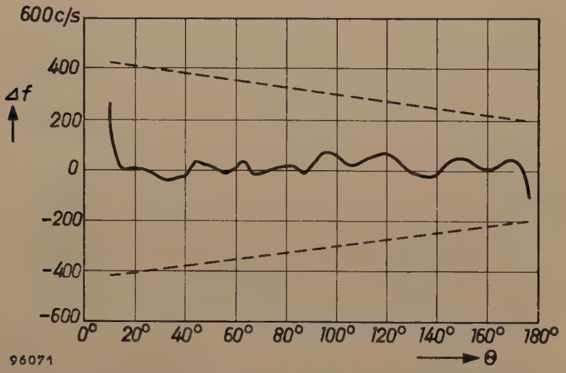

Fig. 9. Typical curve for a linear-law capacitor showing deviations Δf from the straight-line frequency law against angular setting Θ. From 26° to 176° the oscillator frequency passes from 800 kc/s to 400 kc/s. The two oblique dotted lines correspond to frequency errors of ± 0.05%.

The temperature coefficients of capacitance of both versions of this capacitor, i.e., temperature-compensated and non-temperature-compensated, have been given above (see also Table I).

The long-term stability of a number of capacitors has been measured in the laboratory over a period of several years. Periodic measurements of their frequency calibration curves show that these capacitors have a stability of better than ±0.02% in capacitance. Some long-term-stability tests performed by the National Physical Laboratory are shown in *fig. 10a*. The relative humidity at the times of the measurement is shown in fig. 10*b*. The strong correlation between these quantities shows that to minimize capacitance variations desirable to use the capacitor under conditions of low relative humidity. This can be achieved fairly easily by raising the temperature of the immediate surroundings slightly above the ambient temperature, or by dessicating the capacitor enclosure.

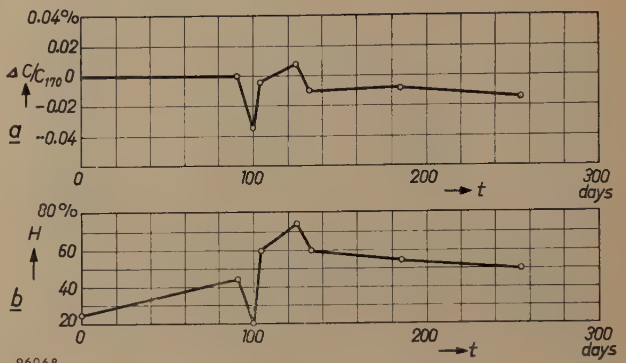

Fig. 10. Uncompensated linear-law capacitor.
a) Variation, over a period of many months, in the *capacitance* swing between the settings 0° and 170°, expressed as a percentage of the capacitance at 170°, measured at 1 kc/s.
b) Corresponding readings of relative humidity *H* taken at the same times as the measurements of $\Delta C/C_{170}$.
It should be pointed out that these variations in capacitance, which are themselves very small, give rise in practice to much smaller percentage *frequency* variations owing to the presence of a parallel capacitance (fig. 3).

Vibration tests carried out over the frequency range between 10 c/s and 150 c/s with corresponding accelerations of 0.2*g*-6.8*g* produce only slight changes in capacitance. In all cases the frequency law remains unaltered well within the specified limits of ±0.05%.

The sine-law capacitor

The accuracy achieved in the sine-law capacitor is ±0.02% of the capacitance swing. Since the latter is about 400 pF (0°-180°, and 180°-360°), the accuracy of the capacitor is within about ±0.08 pF for all angular settings. *Fig. 11* is a graph showing the departure from the ideal law for a typical sine-law capacitor. Also shown in this graph are the specification limits in terms of the frequency (equivalent to ±0.08 pF).

Table II summarizes the properties of this capacitor.

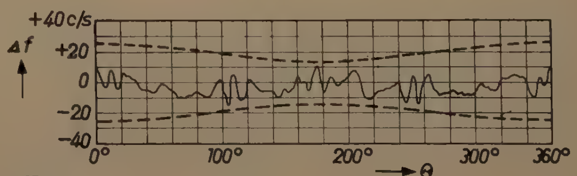

Fig. 11. Deviation Δf in c/s of a typical sine-law capacitor from the ideal sine frequency law, the frequency swing of the oscillator being from 452.32 kc/s to 547.68 kc/s. The dotted lines above and below the curve represent the specification limits (equivalent to ±0.08 pF).

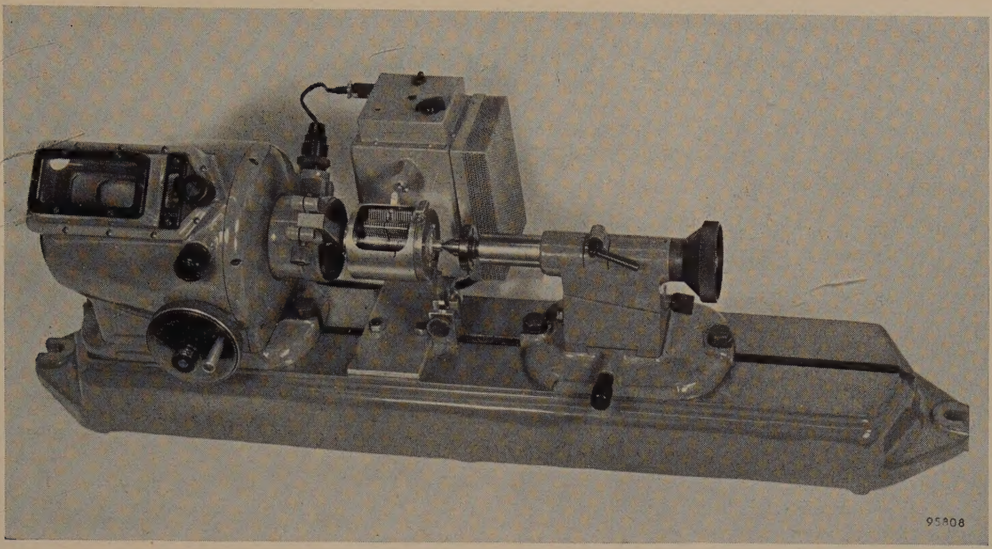

Fig. 12. Precision instrument used for setting angles of the sine-law capacitor. (Optical dividing head by Messrs Precision Grinders Ltd., Mitcham, Surrey, England.)

Measurements have been made to assess the long-term stability of several of these capacitors. These measurements are not easy, however, because of the difficulty in defining the angular position of the shaft of each capacitor. The shaft of this capacitor can rotate continuously, i.e. it has no end stop; it is therefore much more difficult to set up this capacitor to any datum position. In the absence of a mechanical datum, a method of setting-up by electrical means has to be used. The capacitor is mounted on an instrument whose shaft, coupled to the rotor of the capacitor, can be set to any desired angle with a high degree of precision (to approximately 9 seconds of arc). A photograph of this apparatus is shown in *fig. 12*. The shaft is locked to the instrument and the positions (180° apart) at which the circuit gives the same frequency are found experimentally. (Since the law of the capacitor is $f_\Theta = f_m + f_1 \cos \Theta$, there are two positions of the shaft at 90° and 270°, differing by exactly 180°, which give rise to the same oscillator frequency f_m, see *fig. 13.*) Using these two measured angular positions as the datum angles, measurements show that the instability of the capacitors is not greater than ±0.01% of maximum capacitance over periods of up to three months. Periodic measurements have also been made on two capacitors, while actually installed in their equipment, over a period of some eighteen months. No evidence of instability greater than ±0.02% of maximum capacitance has been found over this period.

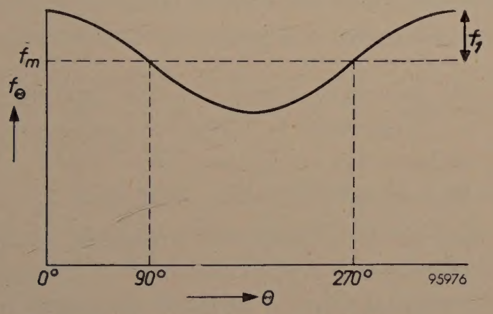

Fig. 13. Indicating the setting of the sine-law capacitor to the two datum positions at 90° and 270° where the oscillator frequency is equal to f_m.

Summary. Two precision variable capacitors are described, one giving a straight-line frequency law and the other a sine frequency law. In order to achieve high accuracy and stability, both capacitors have precision bearings and are mounted in rigid cylindrical cases. The vanes are manufactured from brass sheet machined to close tolerances. The linear-law capacitor has a capacitance variation corresponding to 2 : 1 in frequency, for an angular swing of 26° to 176°. The deviation from the straight-line law is never greater than ±0.05% in frequency. The temperature coefficient of capacitance is about +18 parts per million per °C. Special temperature-compensated versions, however, have a temperature coefficient which is equal to −15 p.p.m./°C. The sine-law capacitor is designed so that its shaft can rotate continuously for long periods. Special attention is therefore paid to the wiper contacts which are of silver-graphite, bearing on a silver slip ring. The capacitance swing (from 0°-180° and 180°-360°) is 398 pF. Conformity to the sine law is within ±0.02% of maximum capacitance. The temperature coefficient is +18 p.p.m./°C. One important use of this capacitor is for the conversion of radar data from polar to cartesian form.

ABSTRACTS OF RECENT SCIENTIFIC PUBLICATIONS BY THE STAFF OF N.V. PHILIPS' GLOEILAMPENFABRIEKEN

Reprints of these papers not marked with an asterisk * can be obtained free of charge upon application to the Philips Research Laboratory, Eindhoven, Netherlands.

2581: A. Claassen and L. Bastings: The extraction of ferric chloride with methyl isobutyl ketone and amyl acetate (Z. anal. Chem. **160**, 403-409, 1958, No. 6).

The extraction of iron as ferric chloride in 7 M hydrochloric acid by a mixture of (1+1) or (2+1) methyl isobutyl ketone and amyl acetate is quantitative for macro as well as for micro amounts of iron. The distribution ratio is very high (~4000). With these mixtures no emulsification difficulties are encountered as they are with methyl isobutyl ketone alone. The behaviour of 44 elements in this extraction has been investigated.

2582: H. O. Huisman, A. Smit and J. Meltzer: Investigations on organic insecticides, I. Preparation and insecticidal properties of some substituted polyenamides (Rec. Trav. chim. Pays-Bas **77**, 97-102, 1958, No. 2).

The preparation and insecticidal properties of a number of substituted polyenamides are described in connection with the occurrence of this type of compound in nature.

2583: H. O. Huisman, J. H. Uhlenbroek and J. Meltzer: Investigations on organic insecticides, II. Preparation and acaricidal properties of substituted diphenylsulphones, diphenylsulphides and diphenylsulphoxides (Rec. Trav. chim. Pays-Bas **77**, 103-122, 1958, No. 2).

The preparation and acaricidal properties of a number of variously substituted diphenylsulphones, diphenylsulphides and diphenylsulphoxides are described. A few of them possess strong acaricidal properties. The most outstanding proved to be 2,4,5,4′-tetrachlorodiphenylsulphone — "Tedion V18" — which combines high activity on all stages, except adult spider mites, with total absence of phytocidal side-effects and toxicity for warm-blooded animals.

2584: T. Kralt, H. D. Moed and J. van Dijk: Ionylamines, I. Synthesis of di- and tetrahydro-α- and -β-ionylamines and their spasmolytic action (Rec. Trav. chim. Pays-Bas **77**, 177-195, 1958, No. 3).

The synthesis and properties of amines and quaternary ammonium compounds with the C-skeleton of ionone and C_{18}-ketone are described. The spasmolytic activities of the compounds were determined. The results are discussed and it is concluded that these series of amines show a high musculotropic spasmolytic activity. The relationship between the chemical structure and the spasmolytic activity in these series of amines is fairly clear and regular.

2585: H. D. Moed, T. Kralt and J. van Dijk: Ionylamines, II. Synthesis of tetra- and hexa-hydro-ψ-ionylamines and their spasmolytic action (Rec. Trav. chim. Pays-Bas **77**, 196-208, 1958, No. 3).

The synthesis and properties of amines with the C-skeleton of ψ-ionone are described. The spasmolytic activities of the compounds have been determined. The results are discussed and the conclusions are reached that the ψ-ionylamines form a series of compounds with high musculotropic spasmolytic activity and that in this series there exists a fairly clear and regular relationship between chemical structure and spasmolytic activity.

2586: H. Koopman and J. Daams: Investigations on herbicides, I. 2-(substituted amino)-4,6-dichloro-1,3,5-triazines (Rec. Trav. chim. Pays-Bas **77**, 235-240, 1958, No. 3).

In view of their herbicidal properties a number of 2-(substituted amino)-4,6-dichloro-1,3,5-triazines were synthesized by a method described in the literature. The influence of the side chain on the herbicidal properties was determined. For this reason some derivatives mentioned in the literature were included to compare them with the new compounds in the authors' biological tests.

2587: M. P. Rappoldt, P. Westerhof, K. H. Hanewald and J. A. Keverling Buisman: Investigations on sterols, X. The conversion of ergosterol and pre-ergocalciferol by U.V. light of 254 mμ (Rec. Trav. chim. Pays-Bas **77**, 241-248, 1958, No. 3).

A study is presented of the conversion of ergosterol and pre-ergocalciferol by U.V. light of 254 mμ. From the experiments certain conclusions are drawn regarding the formation of tachysterol_2 from ergosterol and on the quantum-efficiency of the interconversion of pre-ergocalciferol and tachysterol_2.

2588: H. D. Moed, J. van Dijk and H. Niewind: Synthesis of β-phenylethylamine derivatives, V. Bronchodilators II (Rec. Trav. chim. Pays-Bas **77**, 273-282, 1958, No. 4).

The chemistry is described of three adrenaline-like compounds:

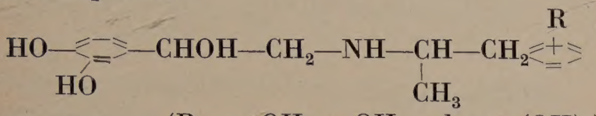

$$\mathrm{HO{-}C_6H_3(HO){-}CHOH{-}CH_2{-}NH{-}CH(CH_3){-}CH_2{-}C_6H_4R}$$

(R = *o*-OH, *m*-OH and *m,p*-$(OH)_2$)

The compounds were examined for their ability to protect guinea pigs from bronchial spasm induced by acethylcholine. The possible influence of the hydroxylated benzene nucleus of the side chain on the drug-receptor combination is discussed.

2589: M. P. Rappoldt, J. A. Keverling Buisman and E. Havinga: Studies on vitamin-D and related compounds, VIII. The photoisomerisations of provitamin-D and its irradiation products (Rec. Trav. chim. Pays-Bas **77**, 327-330, 1958, No. 4).

Results of kinetic investigations and measurements of quantum yields are reported, which cannot be explained by the most simple scheme imaginable for the photochemical interconversions of provitamin-D and its isomers. At least two excited transitory species have to be assumed. More experimental data will be needed before a decision can be made in favour of one or other of the hypothetical, more complicated, pathways.

2590: W. Haidinger: Ein Beitrag zur Kenntnis der brennflecklosen Bogenentladung (Z. Physik **151**, 106-113, 1958, No. 2). (Contribution to the study of arcs without cathode spot; in German.)

For high-pressure xenon discharges with short arcs, it is shown that the transition from an arc with cathode spot to an arc without cathode spot is dependent on the form and emission of the cathode. A special cathode is described for which the transition current under otherwise equal conditions is reduced by about 40%. When this cathode is provided with readily emitting substances, the transition current can be diminished more than 85%. Contrary to earlier experience a re-ignition peak is observed at small currents (low cathode temperature) with this arc.

2591: J. Hornstra: Dislocations in the diamond lattice (Phys. Chem. Solids **5**, 129-141, 1958, No. 1/2).

In this paper several possible structures of dislocations in the diamond lattice are discussed. Special attention is paid to the occurrence of broken bonds in the core of the dislocations and in jogs; for instance, edge-type dislocations can occur in configurations without broken bonds. Jogs can act as a source or sink of interstitials and vacancies; in the diamond lattice this is complicated by the existence of two kinds of atom sites. The most probable types of partial dislocations and the mechanism of their formation from simple dislocations are discussed. In the last section something is said about the occurrence of partial dislocations at twin boundaries and about a line imperfection with zero Burgers vector which may occur at the end of a twin lamella.

2592: J. H. Spaa: A beam-scanned rotating heavy-ice target for high loads (J. sci. Instr. **35**, 175-178, 1958, No. 5).

Of the several possible targets for the $D(d,n)^3He$ reaction the heavy-ice target proves to be the most suitable for outputs of about 10^{10} neutrons per second. Beam scanning in two perpendicular directions combined with rotation of the target is found to be necessary to secure a sufficient life of the ice surface.

2593: F. A. Kröger and H. J. Vink: Relations between the concentrations of imperfections in solids (Phys. Chem. Solids **5**, 208-223, 1958, No. 3).

Imperfect crystals behave statistically like liquid solutions, the crystal being the solvent and the imperfections the solutes. Application of the law of mass action to atomic and electronic reactions taking place in the crystal and between the crystal and the other phases leads to the notion that the concentrations of the various imperfections are interdependent as a result of reactions having partners in common. The consequences of this interdependence are demonstrated by means of a graphical method. Imperfections having opposite effective charges tend to increase each other's concentrations. Foreign atoms are incorporated in a manner dependent both on the energy levels caused by them and on the type of imperfection prevailing in the crystal in the absence of these foreign atoms. In monatomic solids the mechanism of incorporation can be influenced only through the temperature; in compounds it can also be influenced through the partial pressures of the components of the basis crystal. It is shown that the arguments given are valid irrespective of the type of bonding.

2594: G. D. Rieck: Growth and preferred orientations of crystals in tungsten wires (Acta metallurgica **6**, 360-366, 1958, No. 5).

In recrystallized wires of doped tungsten, large crystals have their [421] or [531] axis parallel to the wire axis and small ones tend to keep the original deformation texture [110]. It can be shown that, assuming glide both along $\langle 111\rangle$ and along $\langle 100\rangle$ in the tungsten crystals during drawing, the majority of the crystals attain a [110] texture. However, some crystals which have an orientation near [531] deform on one glide system only. Therefore, during the last stages of drawing, they will tend to turn with respect to neighbouring crystals having a [110] texture. The presence of a dope inhibits the growth of most of the crystals, but least so that of the [531] crystals, as these will have undergone considerable grain boundary slip, resulting in crumbling of the dope skins. Less dope results in more smaller crystals, fewer of which have [531] orientation. The nature of the fragmentation which was already found in the large crystals can be explained on the assumption of tubes or strings of contaminations with blocks and leaks at random places.

2595: J. J. de Jong, J. M. G. Smeets and H. B. Haanstra: Some results of an electron-microscopical study of the metallographic structure of two alloys for permanent magnets (Ticonal G and Ticonal X) (J. appl. Phys. **29**, 297-298, 1958, No. 3).

The microstructures of "Ticonal" G and X in the condition of optimum magnetic properties are studied by the electron microscope using the direct carbon replica. It is argued that a very critical and extensive checking of results is essential in order to arrive at reliable conclusions. Work along these lines demonstrates that *a*) the main structural patterns for "Ticonal" G and X are the same, *b*) the details of the structure of "Ticonal" G and X differ strikingly with respect to texture, width, length-to-width ratio, delineation and intergrowth, and *c*) the influence of the magnetic field during cooling on the structure of "Ticonal" G on a plane $// H_u$ can be shown directly. It cannot yet be decided whether the structure in the optimum condition is a true two-phase structure or a single-phase structure with periodic fluctuations in composition. It is possible that the dimensions revealed by etching do not represent those of the magnetic areas. (Photographs showing the microstructure of "Ticonal" G have appeared in this Review; see Vol. **19**, 11-14, 1957/58.)

2596: A. L. Stuijts and H. P. J. Wijn: Preparation and properties of crystal-oriented ferroxplana samples (J. appl. Phys. **29**, 468-469, 1958, No. 3).

Samples of the hexagonal ferroxplana materials, with a preferential plane for the magnetization, show an increased resonance frequency compared to samples of cubic ferrites with the same permeability. It has been found possible to use the large stiffness for rotation of the magnetization out of the preferential plane, in order to orientate the single crystal particles of a ferroxplana powder in a magnetic field. In this way samples with two different textures have been obtained. In one case the basal planes of the crystals have one direction more or less in common (fan texture); in the other case all basal planes lie more or less parallel to each other (foliate texture). In both cases the permeability is appreciably increased, while the resonance frequency is only slightly decreased. Permeabilities of 56 at 90 Mc/s and 28 at 230 Mc/s, both for $\tan\delta = 0.1$, have been found. This large increase in permeability is caused mainly by an elimination of the effect of the anisotropic permeability of the crystals.

2597: J. Meltzer and F. C. Dietvorst: Action of Tedion on eggs and ovaries of spider mites (T. Pl.ziekten **64**, 104-110, 1958, No. 1).

Eggs of *Tetranychus urticae Koch* of nought to four days of age do not differ in susceptibility to "Tedion". The moment of kill after treatment with "Tedion" is not restricted to a special stage of development. However, most kill occurs between egg stage and nymphochrysalis. "Tedion" affects developing eggs in the ovary of *Tetranychus urticae Koch* after the females have taken up "Tedion" orally. This effect lasts for at least five days after transfer of the females to untreated plants. With CPBS and "Chlorbenside" no complete kill is obtained in this manner, even less than a day after transfer to untreated plants. "Tedion" affects also the developing eggs in the ovary of *Metatetranychus ulmi Koch*. However, in this species the killing effect is lost within two to four days after transfer of the females to untreated plants. "Chlorbenside" acts slightly less in this manner, whereas CPBS is far less active.